DEVELOPMENT OF MICROFLUIDIC PAPER BASED ANALYTICAL DEVICES (μPADS) FOR THE DETECTION OF CALCIUM AND MAGNESIUM IONS

A thesis presented to the faculty of the Graduate School of Western Carolina University in partial fulfilment of the requirements for the degree of Masters of Science in Chemistry.

By

Buddhika Liyana Pathirannahel

Advisor: Dr. Scott W Huffman
Associate Professor of Chemistry
Department of Chemistry & Physics

Committee Members: Dr. Channa De Silva, and Dr. David Evanoff
Department of Chemistry & Physics

April 2018

ACKNOWLEDGEMENTS

First and foremost, I would really like to thank my thesis advisor, Dr. Scott Huffman, who gave me a chance to work with him in the field of microfluidic paper based devices. Not only providing me with guidance but also has been extremely patient with me, when I was going through a difficult time achieving presentable results. Also special thank you to Dr. Channa De Silva for all the support he has provided throughout this journey. Another special thank you to Dr. David Evanoff for the constructive criticism which really helped me to improve and providing with all the encouragements. Special thanks goes to Dr. Carmen Huffman for being so understanding and providing me with guidance with all aspects of graduate school. Wes Bintz and James Cook also deserves a special thank you for always willing to answer any questions that I have. The Department of chemistry and physics always have a special place for providing me with a home away home. A special thanks also goes to the graduate school of research for providing me with all the financial support required.

Sincerest gratitude goes to my parents and my sister for all the support and encouragement you have given me through my entire life and giving me the freedom pursue what I love. Also a very special thanks goes my aunt Dr. Nilmini Abayasinghe. None of this would have been possible without her. And all the rest my family who were there helping me, I thank you!

I cannot thank you enough for all the people that I have met from the moment I stepped to Western Carolina University. To all of my friends who have helped me in any shape or form, no matter how minuscule it is, thank you. Your unwavering support helped me to get through this journey. You all made this my home away from home. Lastly, thank you to Brittni and Alex for always being there for me.

TABLE OF CONTENTS

LIST OF TABLES

LIST OF FIGURES

LIST OF ABBREVIATIONS

μPAD	Microfluidic Paper Based Analytical Device
EDTA	Ethylenediaminettetraacetic acid
EBT	Eriochrome Black T
ICP-OES	Inductively Coupled Plasma Optical Emission Spectroscopy
mM	milli Molar
SCD	Segmented-array Charge-coupled Device
AKD	Alkyl Ketene Dimer
CL	Chemi Luminescence
ECL	Electrogenerated Chemi Luminescence
RGB	Red, Green, Blue
HSV	Hue, Saturation, Value
CMYK	Cyan, Magenta, Yellow, Key
CIE	Commission Internationale de l′Eclairage

ABSTRACT

DEVELOPMENT OF MICROFLUIDIC PAPER BASED ANALYTICAL DEVICES (μPADS) FOR THE DETECTION OF CALCIUM AND MAGNESIUM IONS.

Buddhika Liyana Pathirannahel, Masters of Science in Chemistry

Western Carolina University (April 2018)

Advisor: Dr. Scott W Huffman

Microfluidic paper-based analytical devices (μPADs) have been developed using several patterning technologies to reproducibly create inexpensive lab-on-chip type analytical tools. Consequently, these devices are useful for field deployable measurements in the areas of healthcare diagnostics, environmental monitoring and forensic analysis. These devices are portable, cost effective and easily reproducible. One of the significant characteristics of μPADs is that they are extremely versatile. Thus, they can be modified to any application, particularly in low resourceful settings.

The goal of this project was to create novel microfluidic paper-based analytical devices μPADs that were able to detect and quantify the presence of calcium and magnesium ions in water samples using a simple complexometric titration. The work involved in this project can be divided into two parts. The first part was spent on optimizing parameters that are needed to produce μPAD consistently and repeatedly using wax printing method. The parameters studied are the melting temperature, the melting time and their effect on the barrier width and the channel width. Based on the results that were obtained, μPADs were designed with ten reservoirs in the middle of channels and ten reservoirs at the end of the channels.

The detection of the calcium and magnesium was performed on the μPADs using typical complexometric titrations. Two separate titration reactions were carried out on μPADs that were prepared separately. The first step was to determine the total water hardness which is the total

concentration of magnesium and calcium ions in water. The pH of the μPADs for this analysis was maintained at pH 10 using CAPS buffer. The ten reaction reservoirs contained various amounts of EDTA, whereas a constant amount of EBT was added to all detection reservoirs. When the amount of total calcium and magnesium ions exceeded that of the EDTA in the reaction reservoirs, free metal ions penetrated the detection reservoirs resulting a color reaction from EBT. Therefore, the first detection reservoir with no color change determined the total concentration of calcium and magnesium ions which is equal to total hardness.

Next step was to determine the individual calcium ion concentration at pH 13. The pH on the μPADs was achieved using 10 M KOH. Here the ten reaction reservoirs contained various amounts of EDTA while the detection zone contained a constant amount of calcon as the metal indicator. When a water sample containing calcium and magnesium ions are added to the sample zone, magnesium ions get precipitated as a solid while free calcium ions get penetrated to the reaction and detection zones. Here, the calcium concentration is determined based on the concentration of the first reaction zone with no color change. The effect of other metal ions that might be present in the water on the μPADs were also studied. It was found that the presence of Cu^{2+}, Ni^{2+}, Al^{3+}, Mn^{2+} and Fe^{3+} ions could interfere with the results. The μPADs determined the concentration of metal ions at orders of magnitude ranging from 0 – 90 mM as well as from 0 - 9 mM. The analysis of unknown water samples obtained from the lakes, wells and rivers was also demonstrated in the field using the μPAD, and the results agreed well with those obtained by inductively coupled plasma optical emission spectrometry (ICP-OES).

CHAPTER ONE: INTRODUCTION

Water is an integral part of life. It is used not only for hydration but also for cooking, sanitation, hygiene and many other uses. Availability of safe drinking water is an important aspect of protecting human health. However, urbanization and industrialization have compromised the quality of water across the globe. There are also parts of the world where people are facing a shortage of clean water, therefore, having a significant impact on their health. About 884 million people worldwide are lacking safe water supplies, which is equivalent to one in eight people on the globe.[2] Many of them consume hard water that can contribute to many health issues such as cardiovascular diseases,[3] diabetes,[4] atopic dermatitis,[5] and even cancer.[6]

Water hardness is defined as the total concentration of calcium and magnesium ions dissolved in water. Other divalent or multivalent cations including aluminum, barium, strontium, iron, zinc, and manganese can also cause hardness in water. However, monovalent cations sodium and potassium are not responsible for producing water hardness.

Limestone is one of the significant contributors of calcium ions into the water system while dolomite is the primary source of magnesium ions. Since dolomite and limestone are mostly found in underground, water hardness is generally significantly higher in groundwater than surface water.

With rising populations, the demand for clean and safe water is also increasing. In order to supply the demand of clean water, new policies and safety regulations are being implemented.[7] This involves regular monitoring of water sources across the world. In many developing countries and rural areas, laboratory infrastructure for characterizing these problems is lacking. Since monitoring takes place very often, it is essential that technology used to monitor water quality not only be accurate, but also field-portable, robust, inexpensive and user-friendly. Thus, efforts are underway to develop new analytical tools to address the world's water testing needs including inexpensive paper-based test kits. Although obtaining quantitative data is the most preferred, most

of the commercially available low-cost test materials provide only qualitative data.

1.1 Why microfluidic paper-based devices (μPADs)?

Constructing microfluidic devices using paper as the substrate is being evaluated for a wide variety of diagnostic tests. Microfluidic paper-based analytical devices, commonly known as μPADs are constructed by patterning hydrophilic channels demarcated by hydrophobic barriers. Unlike standard dipstick assays, μPADs have separate regions for sample and reaction zones. This allows the samples to react with different reagents simultaneously in different reaction zones. Further, by adjusting the features on the μPAD, reaction times can also be altered.[8] Accordingly, these devices are designed to achieve four simple capabilities in one analytical device. These capabilities are:

1. the distribution of a sample into multiple regions allowing for numerous analyses or replicating one analysis multiple times,

2. moving of the samples through capillary action without the need of a pump, or other external force

3. the capability of analyzing with small volumes, and

4. the minimal generation of hazardous waste.

Further, developing μPADs do not necessarily require complex machinery. Therefore, the cost of developing μPADs is very minimal, and the fabrication of these devices is relatively simple. One of the greatest advantages of these devices is the versatility of its potential applications. With simple modifications of the reagents and without any external modifications, μPADs can be utilized for a variety of purposes.[9]

1.1.1 Selection of paper as the substrate for μPADs

Cellulose fibers are the main component of paper. These fibers are hydrophilic in nature and allow aqueous solutions to flow easily through capillary action.[10] Following this concept, paper has become a substrate of interest in the field of microfluidics.[11]

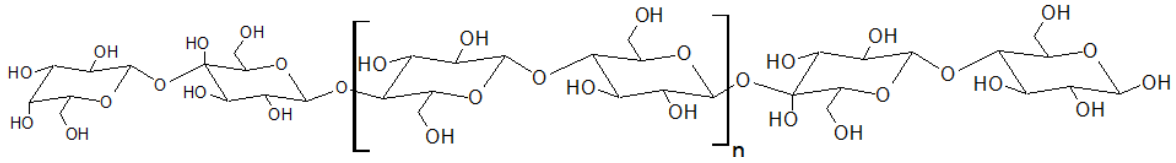

Figure 1. The structure of cellulose (n = degree of polymerization)

As shown in Figure 1, cellulose, which is a polymer of glucose, composed of hundreds to thousands of linearly arranged D-glucose units. The glucose units are connected to one another by β (1,4) glycosidic linkages.[12] The degree of polymerization, depends on the extraction method and the source of material.[13,14] For example, depending upon the method of treatment, the degree of polymerization of cotton could range from 800 to 10000 monomer units.[15]

Paper based products mainly consist of 90 – 99 % cellulose fibers. The typical length, width and wall thickness of a single fiber are about 1.5 mm, 20 μm and 2 μm respectively. Cellulose is different from other polymers due to its polyfunctionality. The long chains provide higher stiffness compared to the other polymers.[15] The network of cellulose in sheets of paper creates pores. These pores allow the liquids to penetrate into the paper. Depending on the capillary pressures, liquids migrate from large pores to smaller pores.[16] Further, cellulose is easily biodegradable, and insoluble in water and the majority of organic solvents. These qualities make cellulose ideal for using as the substrate in microfluidic paper-based analytical devices.[17]

The first commercially available paper based testing stripe, Clinistix, was developed by Free *et al.* in 1956 for detecting glucose.[18] In their study, filter paper was treated with glucose oxidase,

peroxide, and orthotoline. Then, in the presence of glucose, the paper turned blue. This discovery led to usage of paper as the substrate for various other bio-assays.[18]

1.1.2 Portability and user-friendliness of μPADs

Since μPADs are known for their portability to the field, the risk of contamination or degradation of the analyte is significantly reduced. The response time for the analysis is quicker with the use of μPADs. As long as the μPADs are user-friendly and portable, the benefits mentioned above can be applied. Some of the methods that were developed to make μPADs user friendly include using smartphones,[19–24] portable cameras and portable scanners[25,26] as the reading device. For example, Sicard and his group developed a paper based device in conjunction with a smartphone application to provide the organophosphate pesticide concentration in water resources.[22] Usage of a smartphone can be beneficial not only for image capturing, but also for data collection, storage and sharing-on-line in real time.[22] Further, a QR (Quick Response) code containing information about the analyte was developed by Santhiago *et al.*[20] that enabled the smartphone to read μPADs and output data.

1.2 Fabrication methods of μPADs

There are numerous methods available for fabricating μPADs. Each technique has its own benefits and drawbacks.

Fabricating μPADs by wax screen printing method combines standard emulsion-based screens with hydrophobic reagents to create barriers on the paper. This method involves two steps: (1) rubbing solid wax through a screen onto the paper, and (2) melting wax on a hot plate allowing it to get absorbed into the paper.[27] There are several advantages to this method including wide availability of the screen printing technique, environmentally friendliness, and simplicity in fabrication without the need of sophisticated instrumentation; making it ideal to be implemented in developing countries. However, one disadvantage is that the resolution ($\sim$ 850 μm minimal line

width) of these μPADs is very low.[27]

Abe *et al.* demonstrated the use of inkjet printing method to fabricate a microfluidic single use optical sensing device for the quantitative analysis of pH, total protein and glucose.[28] First, to make the filter paper hydrophobic, it was dipped in a polystyrene solution and allowed to dry. Then, printing hydrophilic patterns followed by immobilization of the reagents needed for chemical sensing were done using an inkjet printer. Digital color analysis in the L*a*b* color space was achieved using a color scanner and a computer to get a quantitative reading. As this method uses a single printer to fully develop a microfluidic devices including the application of the reagents, it would be suitable for fabricating and using even in remote locations. This technique is highly efficient, and a regular inkjet printer can be modified to perform this task, however these modifications can be expensive.[29]

Alkyl ketene dimer (AKD) is typically used in inkjet printing of the μPAD. In this technique, once the AKD is applied onto the paper, it is heated to polymerize and create the hydrophobic barriers on the paper.[11] As a non-toxic alternative, UV curable inks can be used instead of alkyl ketene dimer (AKD).[30,31] While the cost of inkjet printing is very low, heating involved in the process can damage the paper.[11]

Whitesides and his co-workers used a photoresist to create μPADs. Photoresist was exposed to UV light through a photomask. This technique is called photolithography.[32] These μPADs exhibit a very high resolution of the barriers. However, the μPADs are not flexible. Furthermore, the cost of chemicals, and their disposal fees are high.[33]

Wax printing is a widely used fabrication technique for developing μPADs.[34] A commercially available printer with wax-based ink is used for printing hydrophobic barriers on the paper. The wax is then melted onto the paper through heating. This technique is simple and rapid, making them ideal for implementation anywhere in the world. Disadvantages to this method include instability of these μPADs at high temperatures due to degradation of wax and paper, and poor resolution of their barrier edges.[34]

1.2.1 Detection methods used in μPADs

In order to make μPADs suitable for using in remote locations, not only the fabrication, but also the detection methods need to be affordable and cost effective. As of now, there are an array of detection methods that can be combined with μPADs to obtain expected results.

Electrochemical detection requires a framework of three–terminals – a working cathode, a counter cathode and a reference electrode. These are imprinted onto paper utilizing conductive inks.[35] Dungchai *et al.*[36] were the first to adapt this technique to paper-based microfluidics to detect glucose, lactate and uric acid in urine. The cathodes were printed onto the μPADs using screen-printing, and cyclic-voltammetry was used for reading the signals given by the electrodes. Some of the advantages of using electrochemical detection in μPADs are lighter-weight, disposability, high sensitivity and accuracy[37] and high response rate that depends on the concentration of analyte.[38] In this particular experiment, once a sample is deposited on to the center of the μPAD, it migrates to the reaction-site with electrodes. H_2O_2 is released when oxidase enzyme reacts with the reactants. The level of H_2O_2 produced was monitored to determine the level of the analyte.

Fluorescence detection involves measuring emission of light in a chemical reaction. Compared to photometric measurements, fluorescence measurements are highly sensitive; as the analyte signal depends on both the intensity of incident radiation and the concentration of the analyte.[39,40] In μPADs, fluorescence detection is mostly reported in measuring fluorescence quenched by the analyte, rather than directly measuring the emission. For example, Wang *et al.* reported measuring fluorescence quenching of CdTe quantum dots (QDs) deposited on glass fiber paper by Cu^{2+} ions, to detect the Cu^{2+} in aqueous samples.[41] Fluorescence direct emission or fluorescence quenching can be detected by commercially available fluorimeters, plate readers that can detect fluorescence or even with the use of mobile camera equipped with a suitable software application.[42] However, commercially available white papers are typically treated with various bright-

ening agents. This can interfere with the fluorescence signal by causing high level of background noise.[17]

Colorimetric detection is the most widely used method of detection in μPAD technology. This method typically involves a color change reaction that can be observed by naked eye.[43] The high versatility of this technique makes it applicable for a variety of analyte detections. These analytes could be biological agents such as glucose, proteins[44] and biomarkers[45] or environmental pollutants such as various metals.[46] Martinez *et al.*[44] used colorimetric detection to identify glucose and proteins in artificial urine. In this experiment, the presence of glucose was determined by the oxidation of iodide to iodine. The oxidation causes a color change of colorless to brown. Protein presence was monitored by the color change of tetrabromophenol blue from yellow to blue.[44]

One of the greatest advantages of colorimetric detection is that it does not require any specific instrumentation.[47] Hence, it is ideal to be used in a low resourceful settings. For colorimetric detection, digital photography or digital scanning is typically utilized to analyze color changes. The intensity of the color changes is analyzed using color analysis software such as ImageJ. The colors can be analyzed as RGB (Red, Green, Blue), CMYK (Cyan, Magenta, Yellow, Key), HSV (Hue, Saturation, Value) or grayscale.[48]

Although colorimetric detection is widely used, there are some drawbacks to this method. Unevenness of illumination while using digital cameras is one of the issues this technique encounter. In order to address this issue, an enclosure or mounting frame is often used. However, even with these adjustments to resolve this problem, the possibility for errors due to color variability is still present. Carrying out multiple replicates of the same reactions will yield better results.[49]

With the introduction of CIE RGB color space in the 1930s, chemists established the use of color reactions for quantitative analysis.[50] This expertise can be applied to new technologies and substrates to make suitable test kits. Thus, in the present work, colorimetric detection through the color change of metal-complexometric titrations were utilized and brought over to a paper based

substrate to develop a lab on a chip type microfluidic device.

1.3 Using μPADs for water analysis

In addition to soluble metal ion carbonates, water in natural reservoirs contains many other chemicals. For example, aquatic photosynthesis thrives on nitrogen and phosphorous. However, due to the release of agricultural and waste water without any treatments, the levels of phosphorus and nitrogen have increased in the recent years. Therefore, μPADs can be used effectively in water analysis for monitoring ammonia, nitrates, nitrites and phosphates levels.[7]

Nitrates and nitrites can cause severe health problems such as gastric cancer and methemoglobinemia.[51] Several μPADs were developed by stamping, inkjet printing and paper cutting for detecting nitrates and nitrites using the Griess reaction[19,52,53] and s-tetrazine chemistry.[21] Phosphates were determined by μPADs that used the molybdenum blue reaction.[54,55] Heavy metal ions in large concentrations can be detrimental to the health of both humans and animals. Most of these heavy metal ions tend to accumulate in waterways over time.[56]

High Hg^{2+} levels can lead to kidney and brain failures. Also accumulation of mercury in water ways could lead to mercury being converted to toxic form by aquatic bacteria.[56,57] To determine the mercury levels in water, μPADs were developed by using either colorimetry or electrogenerated chemiluminescence (ECL).[58]

Industrial waste waters can contain elevated levels of chromium, copper, lead, nickel, and zinc ions which ultimately could end up in freshwater bodies. In order to determine the concentration of Cr^{6+} present in water, μPADs were developed by using the plasmon resonance of bovine serum albumin-capped gold nanoparticles for colorimetric detection.[59] Alahmad *et al.* developed a detection method to test chromium (III) using chemiluminescence (CL) in waste water.[60]

μPADs were also developed using fluorescence[41] or colorimetry[61–65] for the determination of Cu^{2+} in water samples. Some of the reagents that have been used in colorimetric methods include

chromogenic reagents,[61] polymer inclusion membranes treated with a chromogenic reagents[62] and silver nanoparticles.[63]

Iron is another common heavy metal ion that can be found in water. Despite being considered a micronutrient, high levels of iron can affect the quality of crops treated by iron-rich water. In waterways, iron exists as both Fe^{2+} and Fe^{3+} ions depending on the pH level of the water. When μPADs are used for iron detection, phenanthroline is used as the reagent. In this reaction, Fe^{2+} ion forms an orange-red complex with phenanthroline to provide a color change from colorless to orange-red.[66]

In general, μPADs have the capacity to detect multiple analytes simultaneously. For example, Ujwar *et al.* developed a μPAD to visually detect the presence of Hg^{2+}, Co^{2+} and Zn^{2+} ions within one device.[67] Further, development of advanced μPADs to measure multi-parameters using colorimetric, electrochemical and ECL detection methods was also reported. For example, detection of Cu^{2+} ions by colorimetry; Cd^{2+} and Pb^{2+} through electrochemical detection;[65,68] and Hg^{2+} and Pb^{2+} ions by ECL detection methods were done using μPADs.[58]

Kaneta *et al.* reported the use of μPADs for the complexometric titrations of Ca^{2+} and Mg^{2+} ions in natural water.[69] The μPAD was designed to quantitatively measure the total hardness of water using colorimetric methods through complexometric titrations. Although the study describes and reports measuring the total Ca^{2+} and Mg^{2+} ion concentrations (total hardness) in water, detailed information and data for measuring the individual Ca^{2+} concentration in water is lacking.

1.4 Development of μPADs for analyzing hardness of water

In the present work, developing μPADs for detecting total water hardness as well as individual Ca^{2+} and Mg^{2+} ion concentrations in unknown water samples is further developed. Hardness of water is simply defined as the total amount of dissolved calcium and magnesium ions in water. In addition, although their concentrations are usually very minor compared to Ca^{2+} and Mg^{2+}

ions, several other dissolved metal ions including aluminum, barium, strontium, iron, zinc, and manganese etc. are also responsible for the total hardness. According to general guidelines, hardness of water can be classified using the concentration of calcium carbonate in water: (1) 0 – 60 mg/L soft; (2) 61 - 120 mg/L moderately hard; (3) 121–180 mg/L hard; and (4) $>$ 180 mg/L as very hard water.[70]

Mineral deposit formation in pipes and boilers *etc.* is a commonly known issue with hard water. This precipitate which is also known as scale takes place due to an ionic reaction. When hard water gets heated, Ca^{2+} ions react with CO_3^{2-} ions to form an insoluble precipitate $CaCO_3$. This is an insoluble precipitate which can clog dishwashers, pipes *etc*. and water flow can be affected.

In addition, it was also found that drinking hard water is connected to cardiovascular diseases including growth retardation, reproductive failure, and other health problems.[71] Thus, knowing the total hardness as well as separate concentrations of Ca^{2+} and Mg^{2+} ions in water is useful.

Water hardness can be measured in several ways including potentiometric and colorimetric methods. In colorimetry, classic titration methods are used for the determination of the water hardness. These classical methods allow to determine the total and individual magnesium and calcium ion levels present in a given sample. Typically, the water hardness titration is conducted at a pH 10 to determine the total hardness. Then, another titration is performed at pH 13 which allows for the determination of calcium ion concentrations. The magnesium ion concentration is determined by the difference between the 2.

Cations are capable of making complexes with many substances with a pair of unshared electrons, usually with molecules with N, O, S, fulfilling the coordination number of the metal. When forming such complexes, metal ion is the electron pair acceptor, acting as a Lewis acid. The complexing agent which is the electron pair donor, acts as the Lewis base.[72]

In order to be used in a complexometric titrations, the complexing agent should have the ability to form a well defined single stoichiometric complex. Ligands with two or more complexing groups which have the ability to complex with metal ions are called chelating agents. The titra-

tions performed using a chelating agent are called complexometric titrations.[73]

Herein, these known titrations are the basis for the colorimetric detection of Ca^{2+} and Mg^{2+} ions in a water sample. Here, the back titration of Ca^{2+} and Mg^{2+} ions with Ethylenediaminetetraacetic acid (EDTA) was used. Free metal ions were detected using metal ion indicators Eriochrome Black T (EBT) and 2-Hydroxy-1-(2-hydroxy-1-naphthylazo)naphthalene-4-sulfonic acid sodium salt (Calcon) at pH 10 and 13 respectively, using buffers to maintain the pH values.

EBT in free form at pH 10 is blue. The calcium-EBT complex is a weak complex, thus would not be suitable for determining the concentration of calcium by itself. However, in a mixture of calcium and magnesium ions, EBT reacts with magnesium ions to make a stable complex (Mg-EBT) which is red in color providing a sharp, easily distinguishable color change.[74] Thus, in the current research, in order to determine the total hardness of water at pH 10, EBT was selected as the indicator. In the next step, to determine the concentration of calcium ions, the magnesium ions can be precipitated to $Mg(OH)_2$ at pH 13. At this pH, another metal ion indicator calcon, was used as it imparts a blue color at pH 13. Ions flow to the detection zones and react with calcon indicator to make Ca-Calcon complex yielding a sudden color change to red. Calcon was used as the metal ion indicator at pH 13 because it changes from blue to red when complexed with Ca^{2+}.

In complexometric reactions, the stabilities of the metal–EDTA complexes as well as the metal-indicator complexes strongly depend on the pH of the reaction medium. Thus, controlling the pH to increase accuracy and selectivity is highly important, which can be achieved by buffering the reaction system. However, care must be taken to use buffers which are not strong metal-chelating agents.

Mentele *et al.* described the use of acetic acid/NaCl buffer (pH 4.5) for developing a μPAD using colorimetric assays to detect the particulate metals in aerosols including Fe, Ni, and Cu.[46] Also, in another study in which μPADs were used for quantitative analysis of Hg^{2+} ions, a buffer system using phosphoric acid, acetic acid and boric acid combined with NaOH was used to main-

tain pH 9 which was considered to provide the best color resolution.[75]

1.5 Objective

The overall goal of this research was to develop an optimized μPAD for measuring the calcium and magnesium ion concentrations in water samples. This work specifically evaluates the size, width, and the shape of the μPAD design, the reagents used in the detection of the analytes, strategies for usage, and performance of the μPADs.

CHAPTER TWO: EXPERIMENTAL

2.1 Materials

Standard metal ion solutions were prepared using magnesium sulfate (American Bioanalytical); calcium chloride dihydrate (Fisher Scientific, Waltham, MA, USA), aluminum sulfate (Sigma Aldrich, St. Louis, MO, USA); copper (II) nitrate, nickel (II) nitrate, manganese (II) chloride and iron (III) chloride (Fisher Scientific, Waltham, MA, USA. They were used without further purification.

Ethylenediamine Tetraacetic Acid, Disodium Salt Dihydrate (EDTA) was purchased from Fisher Scientific, Waltham, MA, USA and was used as received. The metal ion indicators Eriochrome Black T (EBT) (MP Biomedicals) and Calcon (1-(2-hydroxy-1-naphthylazo)-2-naphthol-4-sulfonic acid sodium salt) (Acros Organics) were used without further purification.

Buffer systems 0.5 M N-cyclohexyl-3-aminopropanesulfonic acid (CAPS) (Alfa Aesar, Ward Hill, MA, USA), capsules of sodium carbonate /sodium bicarbonate (Cole-Parmer), sodium tetraborate (Sigma-Aldrich), and potassium hydroxide (Fisher Scientific, Waltham, MA, USA) were used without further purification.

Solvent UV-HPLC grade methanol and concentrated nitric (Aldrich, St. Louis, MO, USA) were used without further purication. Ultrapure water with nominal resistivity of 18 MΩ cm (at 25 ^{o}C) from a Milli-Q water filtration system (Millipore) was used throughout the experiments without further treatments.

A series of unknown water samples from local water sources were tested for calcium and magnesium concentrations. The water samples were collected from Scotts Creek (Sylva, NC), South River (Sylva, NC), well water (Sylva, NC), Lake Dillsboro (Dillsboro, NC) and Laurel Oaks (Cullowhee, NC). A commercial water sample, Gerber Pure purified water (Gerber, USA), was purchased from Walmart grocery store in Sylva, NC.

Larger volumes (greater than 1 mL) were pipetted using glass pipettes and smaller volumes (less than 1 mL) were pipetted using micro pipettes (Rainin Classic^{TM} manual single-channel pipette (Mettler-Toledo *Intl.*). These have been calibrated by calibration service personnel and were used without further modifications. The volumetric flasks with calibrated markings were used to determine a specific volumes and used without further modifications.

2.2 Methods

2.2.1 Preparation of EDTA solutions

EDTA solutions varying from 10 mM – 90 mM were prepared by initially making a 100 mM stock solution. The 100 mM solution was prepared by dissolving 9.306 g of EDTA with ultrapure water in a 250 mL volumetric flask. In order to prepare 10, 20, 30, 40, 50, 60, 70, 80 and 90 mM solutions, 5, 10, 15, 20, 25, 30, 35, 40 and 45 mL of the stock solution were added to different 50 mL volumetric flasks. Then, they were diluted up to the mark with ultrapure water to get the specified concentrations.

To get a series of EDTA solutions with concentrations ranging 1- 9 mM, a stock solution of 10 mM was prepared by dissolving 0.941 g of EDTA and diluting with ultrapure water up to the 250 mL mark of a volumetric flask. Then, the EDTA solutions with 1, 2, 3, 4, 5, 6, 7, 8 and 9 mM concentrations were prepared by pipetting 5, 10, 15, 20, 25, 30, 35, 40 and 45 mL respectively of the 10 mM stock solution into nine separate 50 mL volumetric flasks and diluting with ultrapure water to the mark.

2.2.2 Preparation of indicator solutions

The indicator EBT solution was prepared by dissolving 0.100 g of EBT in 10 mL of HPLC-UV grade methanol in a 100 mL Volumetric flask. Once the solid was completely dissolved, it was diluted up to 100 mL with methanol to get a 0.1 % (w/v)solution.

The indicator calcon solution was prepared by dissolving 0.100 g of calcon in 10 mL of 1 M

KOH solution in a 100 mL volumetric flask. Once all the calcon got dissolved, it was diluted with 1 M KOH up to the 100 mL mark to get 0.1 % calcon solution.

2.2.3 Preparation of standard metal ion solutions

All testing and calibration solutions were prepared by making dilutions from a prepared stock solution. In order to test the μPAD with known Ca^{2+} and Mg^{2+} ion solutions, standard calcium and magnesium ion solutions were prepared. The stock solution of calcium ions was prepared by dissolving 18.370 g of calcium chloride dihydrate with ultrapure water in 250 mL volumetric flask. The Mg^{2+} stock solution was prepared by dissolving 30.811 g of magnesium sulfate heptahydrate with ultra-pure water in a 250 mL volumetric flask. The molarities of these stock solutions were 0.5 M. In order to achieve 30 mM and 10 mM concentrations, 6 mL and 2 mL of Mg^{2+} and Ca^{2+} stock solutions were pipetted into two different 100 mL volumetric flasks, diluted with ultrapure water.

A mixture of calcium and magnesium ions was also prepared by measuring 6 mL of 0.5 M calcium chloride stock solution and 6 mL of 0.5 M magnesium sulfate stock solution into a 100 mL volumetric flask and diluting with ultrapure water. The final solution has 30 mM of equal concentrations of Ca^{2+} and Mg^{2+} ions (total cationic concentration of 60 mM).

For the interference analysis, various concentrations of Cu^{2+}, Ni^{2+}, Al^{2+}, Mn^{2+} and Fe^{2+} ion solutions were prepared starting with 100 mM stock solutions. For making 100 mM stock solutions of each metal, 1.1629 g of copper (II) nitrate, 1.4549 g of nickel (II) nitrate, 1.3519 g of ferric chloride, 0.9904 g of manganese chloride and 1.710 g of aluminum sulfate were dissolved in separate 50 mL volumetric flasks and filled to the mark with ultrapure water. The prepared stock solutions were used to make 1, 10 and 50 mM solutions. The solutions were prepared by pipetting 0.5, 5 and 25 mL into separate 50 mL volumetric flasks and up to the mark diluting with ultrapure water.

2.2.4 Preparation of buffer solutions

The sodium carbonate/sodium bicarbonate buffer solution to be tested at pH 10 was prepared as follows. The sodium carbonate/sodium bicarbonate buffer was prepared as a solution by dissolving one capsule in a 100 ml volumetric flask and diluting up to the mark with ultrapure water.

Sodium tetraborate buffer was prepared by combining 0.025 M sodium tetraborate and 0.1 M sodium hydroxide solutions. First, the 0.025 M sodium tetraborate solution was prepared by dissolving 0.956 g of sodium tetraborate in a 100 mL volumetric flask with ultrapure water. The 0.1 M sodium hydroxide solution was prepared by dissolving 0.201g of sodium hydroxide in a 50 mL volumetric flask with ultrapure water. The buffer was prepared by combing 36.6 mL of 0.1M NaOH with 100 mL of 0.025 M sodium tetraborate solution in a beaker.

2.2.5 Preparation of μPADs for testing buffer systems

For testing the suitability of three buffer systems described in section 2.2.4 to be used at pH 10, separate μPADs were designed with each of the buffer systems as follows. First, 60 μL of a buffer solution was added to the center of the μPAD allowing it to spread evenly to the entire hydrophilic area. After the μPAD with the buffer air dried, 2 μL of EDTA solutions (10 mM - 90 mM) were added to the 10 reaction zones, and 1 μL of 2 % EBT solution was added to each of the 10 detection zones. The EDTA solutions were added with 0 mM at the very first position at the top and subsequent concentrations in adjacent zones by going in a counterclockwise manner. The highest concentration of EDTA was added to the last 9 th zone. The EDTA and EBT were added to the zones using micro pipettes. Once all the reagents were completely dry, the μPAD was ready for testing.

2.2.6 Screening the design parameters for μPAD design

The microfluidic structures for the temperature, time, barrier and channel width analyses were created using MS Word. The design of the optimized final μPAD was created using Octave software on the computer. In order to create microfluidic patterns on the paper, a 8.5 in.$\times$ 11 in. of Whatman No.1 filter paper was fed into the Xerox ColorQube 8580N wax printer, and nine μPADs were printed per paper. The wax based ink, ColorQube 8570 Black Solid Ink (Xerox, USA) with the composition of 50 – 60 % paraffin wax, 10 – 20 % resin and 20 % black pigments, was used for printing the microfluidic devices. The printer settings were set to default for letter printing.

Upon heating, printed wax creates hydrophobic barriers on the paper. A hot plate was used to create hydrophobic barriers by melting the printed wax so it penetrated to the back side of the paper. Aluminum foil was placed between the paper and the hot plate surface to control contamination of the μPAD.

The temperature of the hot plate given by each knob setting was determined by the following procedure. First a beaker with a block of paraffin wax was placed on the hot plate, and dialed to a predetermined knob setting. Then, a digital thermometer was inserted in to the melted wax in the beaker, and kept until the temperature remained constant. Then measurement was recorded as the corresponding temperature for that specific dial. The same procedure was repeated to the remaining dial settings on the hotplate to get the corresponding temperatures.

In the channel width analysis, 5 μL of red food coloring was added to one end of the channel and the distance it travelled at 10 seconds was measured. The time was taken using a stopwatch without further modification. A video camera was used for capturing the distance that the colored water travelled in the microfluidic channels. A ruler with 0.1 mm increment was aligned next to the channel. The videos were stopped at 10 seconds and the distance travelled was measured.

2.2.7 Optimized design, fabrications and standardization of the μPAD

As shown in Figure 14, the design is circular and the outside diameter is 51 mm. The diameter of the middle circle where the sample is applied is 15 mm. The channel lengths from the middle to the reactions zones and reaction zones to the detection zones are 4 mm and 8 mm respectively. The diameter of the reaction zone and detection zone is 3 mm. The μPADs were printed as 9 per page and then were cut into individuals. Then each μPAD was heated on a hot plate to get the wax to form hydrophobic barriers. Then, one side of the heated μPAD was sealed with parafilm. The black background is the hydrophobic barrier of the white design.

As shown in Figure 14, the μPADs with detection zones of 0 – 9 mM or 0 - 90 mM range were prepared as follows. The individual μPAD for testing total water hardness was prepared by adding 80 μL of 0.5 M CAPS buffer solution to the center, and allowing it to spread evenly to the entire hydrophilic area. After letting the μPAD with the buffer to completely air dry, 2 μL of EDTA solutions (0 – 90 mM or 0 – 9 mM EDTA as described in section 2.2.1) were added to the 10 reaction zones counterclockwise and 1 μL of 2 % EBT solution was added to each of the 10 detection zones using micropipettes.

In order to determine calcium ion concentration, a μPAD for titrating at pH 13 was prepared as follows. To a μPAD with the design as of Figure 14, 8.3 μL of 10 M KOH solution was added to the sample zone. Once the KOH solution was completely dry in the center, 1 μL of EDTA solutions (0 - 90 mM or 0 9 mM EDTA as described in section 2.2.1) were added onto the reaction zones counterclockwise and dried at room temperature for 30 minutes. Then, 1 μL of calcon was added to the detection zones and let it dry for another 10 minutes. These μPADs (Figure 19) are able to quantify of 0 - 90 mM or 0 - 9 mM Ca^{2+} concentrations, and they were stored in vacuum sealed desiccators until they are ready to use.

2.2.8 Inductively Coupled Plasma Optical Emission Spectrometer ICP-OES

An Inductively Coupled Plasma Optical Emission Spectroscopy spectrometer (ICP-OES) was used to externally validate the μPAD results from unknown samples. The measurements were recorded using a Perkin Elmer Optima 4100 DV ICP-OES equipped with a Segmented-array Charge-coupled Device (CCD). The CoolFlow CFT-75 temperature was set to 20 $\pm$ 1 ^{o}C. The flow rates of plasma gas were 15 L/min, auxiliary gas flow was 0.2 L/min, and nebulizer gas flow was 0.8 L/min along with peristaltic pump flow rate of 1.5 mL/min. Each of the sample scans were run in triplicates.

2.2.9 Standard and sample preparation for ICP-OES

To dilute the samples, 2 % nitric acid solution was prepared by dissolving 20 mL of concentrated nitric acid in a 2000 mL volumetric flask using ultrapure water. A 50 ppm calcium and magnesium stock solution was prepared by dissolving 0.0126 g of calcium nitrate and 0.0122 g of magnesium chloride dihydrate with 2 % nitric acid in a 250 ml volumetric flask. The measured solids were initially dissolved with 10 mL of the 2 % nitric acid. Ten solutions with concentrations of 0.5, 1, 2, 3, 4, 5, 6, 7, 8, and 9 ppm were prepared using the 50 ppm stock solution by pipetting 0.5, 1, 2, 3, 4, 5, 6, 7, 8 and 9 mL of the stock solution into 10 different 50 mL volumetric flasks and diluting to 50 mL with 2 % nitric acid. For ICP-OES analysis, 15 mL of each of these solutions was transferred to seperate 15 mL conical tubes.

In order to prepare the unknown water samples for ICP-OES analysis, they were diluted with nitric acid. From the unknown water sample, 1 mL was pipetted to a 10 mL volumetric flask and diluted with 2 % nitric acid to get a 10 % diluted sample.

CHAPTER THREE: RESULTS AND DISCUSSION

3.1 Optimization of wax melting temperature (wax flowing temperature)

The melted wax should penetrate all the way to the other side in order to get a hydrophobic surface that spans the thickness of the paper. To optimize the temperature for melting the wax, hollow rectangles with outer dimensions of 34.32 $\times$ 6.21 mm and wall dimension with 2.5 mm were printed on the paper. This shape was chosen as a simulation of the μPAD channels. Then, a hot plate was set to a specific temperature, and the wax was melted through the paper for 60 seconds. After melting, the front and back barrier widths of the rectangles were measured using a vernier caliper. In Figure 2 is shown a picture of the hollow rectangles.

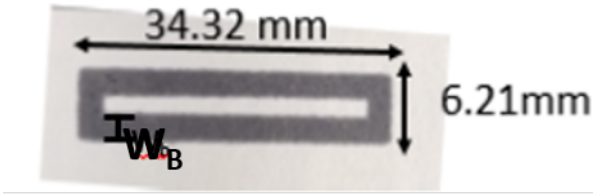

Figure 2. Illustration of the rectangular shape that was used for determining the best temperature for melting wax.

For each temperature, five rectangles were printed and melted, and the three barrier widths (W_B) of each rectangle were measured in the front and on the back at approximately the same locations. The measurements were made along black lines (W_B) at three different locations at approximately at 1/4, 1/2, 3/4 along the channel length. In Figure 3, the barrier width of the front and back vs heated temperature is plotted. This graph shows that the barrier width for front and back increases with increased temperature, and then it decreases.

Using the data from Figure 3, the difference of barrier widths from front to back were calculated. In Figure 4 is shown a graph of the differences between the front and back barrier widths.

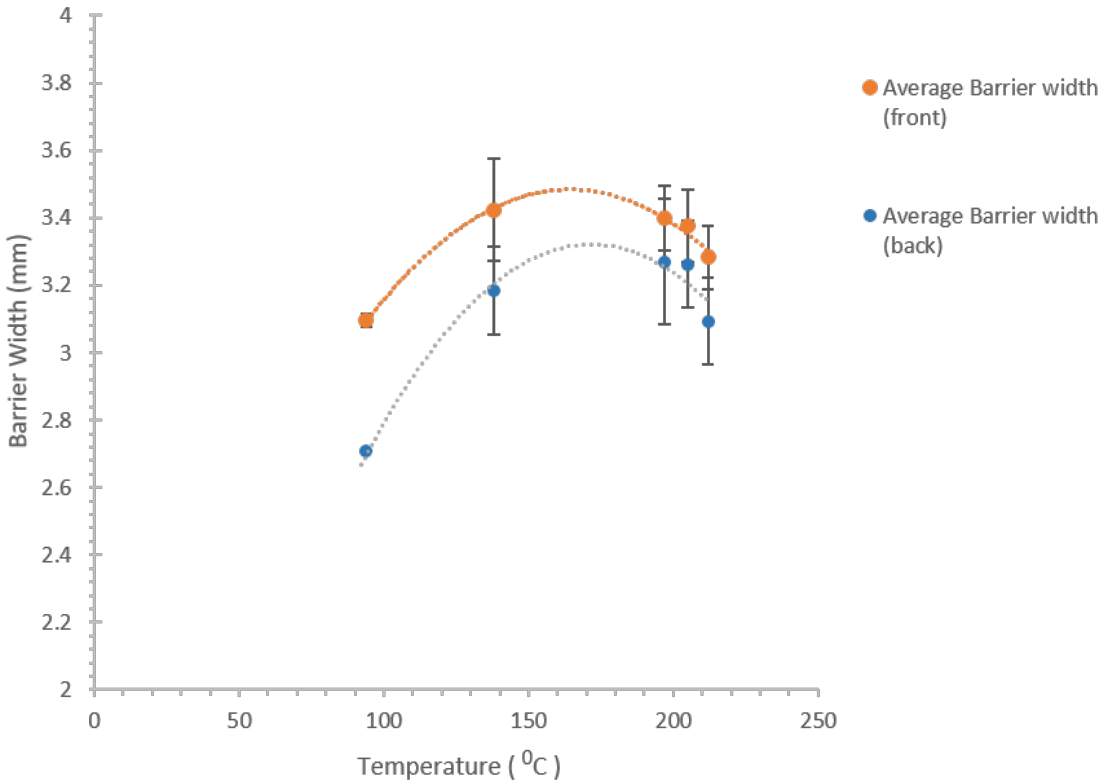

Figure 3. The barrier width of the front and back vs heated temperature. The blue line is the barrier width on the front side of the paper and the orange line represents the barrier width on the back of the paper.

The barrier width difference between the printed and non-printed sides of the paper shows a dependence on the barrier width as a function of temperature.

Below the melting temperature of the wax, there is no movement of the wax toward the non-printed side of the paper. So the difference is the same size as the printed side of the barrier, and therefore meaningless.

Above the melting temperature of the wax, as illustrated in Figure 5, it can spread both through the thickness of the paper as well as laterally across the paper at different rates. In paper construction, fibers are aligned more horizontally than vertically making the paper anisotropic.[34] Wax spreading happens along the length of the fibers more readily (lateral spreading only) than

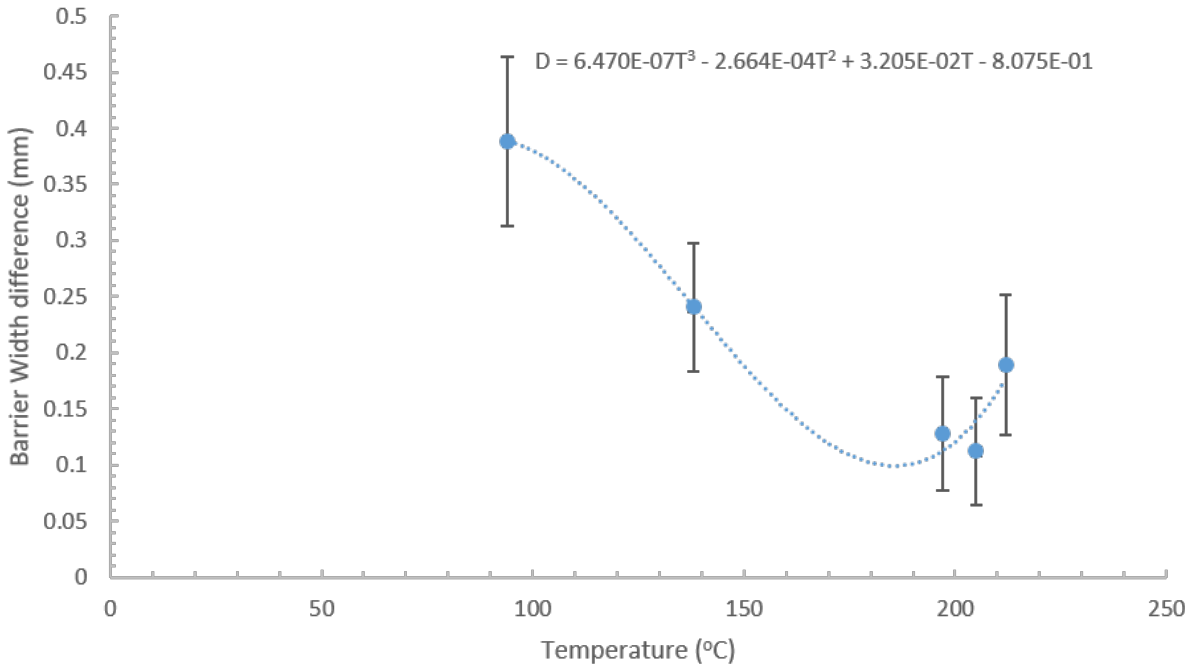

Figure 4. The barrier width difference from front to back vs heated temperature.

between fibers (lateral and vertical spreading).[76] When the wax flow rate is greater in the lateral direction than the vertical direction, the barrier widths on the printed and non-printed sides will be different resulting in a trapezoidal barrier cross-section. At temperatures near the melting point of the wax, the viscosity of the wax is low, which results in slower wax flow rates. At higher temperatures, well above the melting temperatures, the wax flow rates are greater, and at a short enough flow time (discussed in Section 3.2), the resulting barrier width differences are minimized.[34]

The upturn of the barrier width differences above 150 ^{o}C, as shown in Figure 4, is attributed to loss of wax at the paper surface nearest the hot plate (non-printed side). Above 150 ^{o}C, smoke was observed, which could be due to evaporation or degradation of the wax. These results are in agreement with the literature. For example, Dungchai *et al.* reported, in a smaller μPAD than the one described herein, that the barrier width is a function of temperature.[27] They tested heating

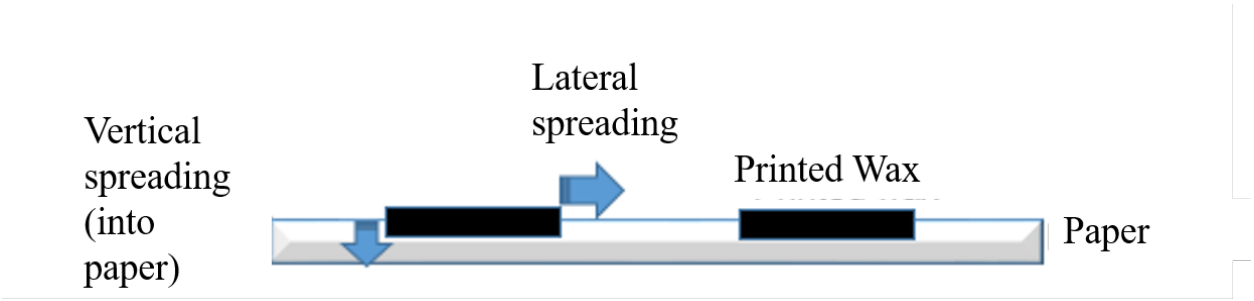

Figure 5. Possible ways of wax spreading on a paper substrate when heating. It can spread along the length of the fibers and between fibers.

durations of 50 s and 60 s at 100 ^{o}C, 150 ^{o}C and 10 s at 200 ^{o}C, and found that the barrier width increases with the temperature increase.

The data in Figure 4 was fitted with a cubic function in MS Excel shown in equation 1

$$D = 6.47 \times 10^{-7}T^3 - 2.66 \times 10^{-4}T^2 + 3.20 \times 10^{-2}T - 8.07 \times 10^{-1} \quad (1)$$

Where, D is the barrier width difference, and T is the heated temperature. The minimum of the function in equation 1 was determined using the 1^{st} derivative, and was found to be at 186 ^{o}C.

Unfortunately, at temperatures above 150 ^{o}C, smoke was visible emanating from the samples, which is attributed to degradation of the wax. Therefore, the temperature 140 ^{o}C was selected for the optimal wax melting temperature in the μPADs.

3.2 Determination of the duration needed for melting wax

Dungchai *et al.* also tested heating duration ranging from 10 - 40 s at 100 ^{o}C and 150 ^{o}C, and found those times not to be effective.[27] In order to determine the duration of the heating, a rectangular microfluidic structure as shown in Figure 2 was heated at 140 ^{o}C for various durations and the barrier width of the printed and non-printed sides were measured with a calliper.

In Figure 6 is shown the barrier widths of the printed and non-printed sides. The barrier widths

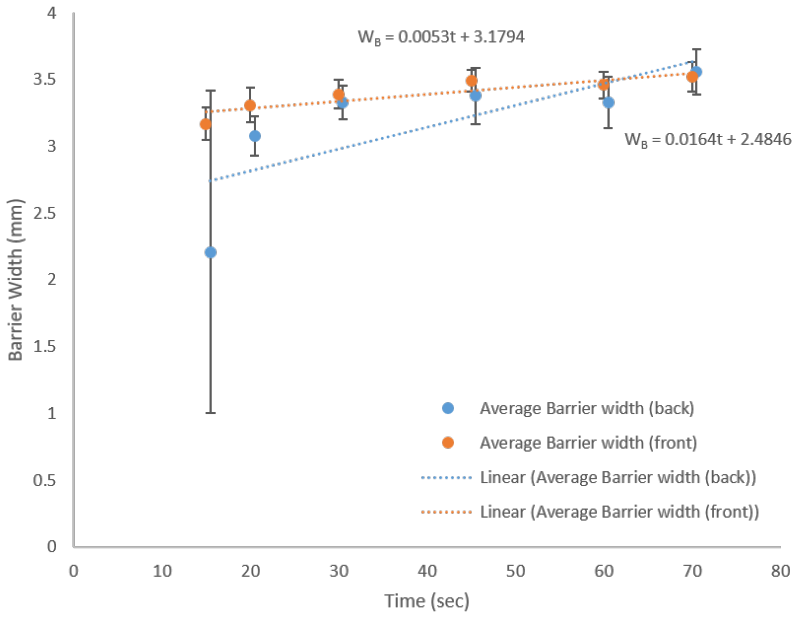

Figure 6. Heating time vs the front and back barrier width of the rectangular microfluidic structure (Figure 2). Orange circles represent the front barrier width and blue circles represent the back barrier width of the structure after heating for the specified time.

for printed and non-printed sides increase with increasing time. At the intersection of the two linear fits of the two data sets the barrier widths are the same. The intersection of the two linear fits was solved algebraically and found to be 62.5 seconds, which was rounded to 60 seconds for ease of timing.

At 20 seconds the variation in back barrier width is the highest (lowest blue point), because duration is not quite long enough for the wax to reproducibly reach the non-printed side of the paper. It was determined that heating the μPAD for 60 seconds would be a sufficient time for the wax to penetrate completely to the back side and form equal width barriers on both sides of the paper. In the literature, the duration of heating wax printed μPADs are also close to 60 seconds.[27]

3.3 Determination of the relationship between printed channel width and melted channel width

In order to determine the relationship between the printed channel width and melted channel width, a set of experiments were performed. In Figure 7 is shown a diagram of the cross-section of the paper both after printing and after melting. The dark black lines with defined widths of W_{P1} and W_{P2} shows the original width of the printed lines. The inner distance of the printed lines is defined as W_G.

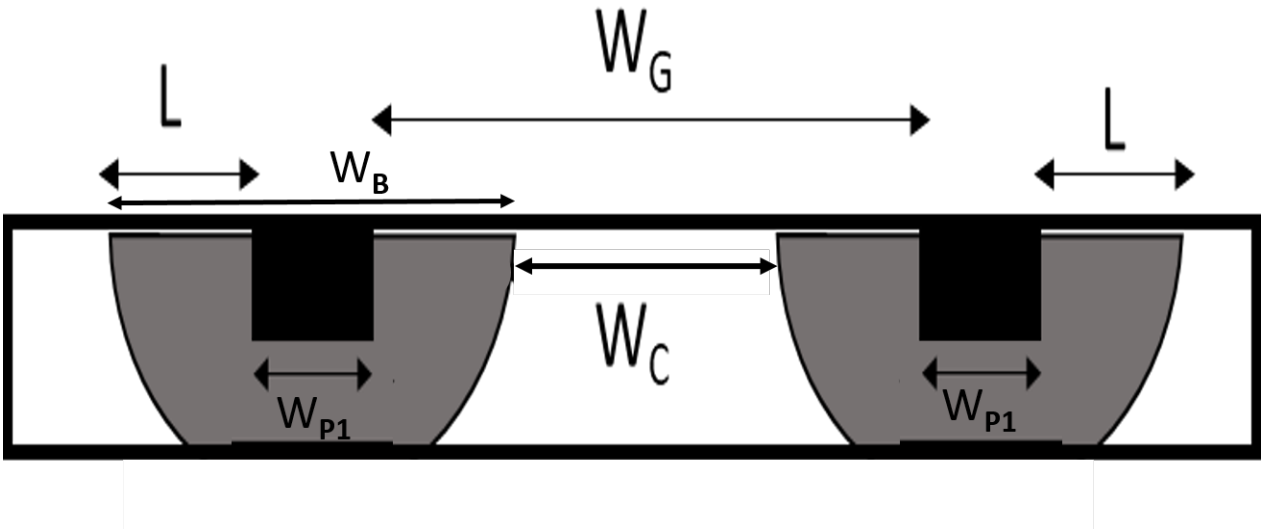

Figure 7. Illustration of the spreading of printed wax on chromatography paper and definitions of the factors for defining PADs. W_G is the distance between printed width which is the gap between the printed lines prior to heating; W_B is the Barrier Width; W_{P1} and W_{P2} are the printed widths; W_C is the channel width which is the inside width after heating. The black rectangles represent printed area, and gray area shows where wax spread after heating.

After melting, wax spreads a distance of L, ideally in both directions, which narrows the space between lines. The resulting inner distance between the melted lines is defined as channel width W_C, which is the hydrophilic channel where the aqueous solutions flow. The widths of the lines after heating are defined as barrier width W_B.

As mentioned in sections 3.1 and 3.2, the optimized temperature and time to get barrier width

of front and back of the paper with least difference was determined to be 140 ^{o}C and 60 seconds, respectively. In order to determine the effect of printed width on barrier width, a study was performed using a series of samples with varying line widths.

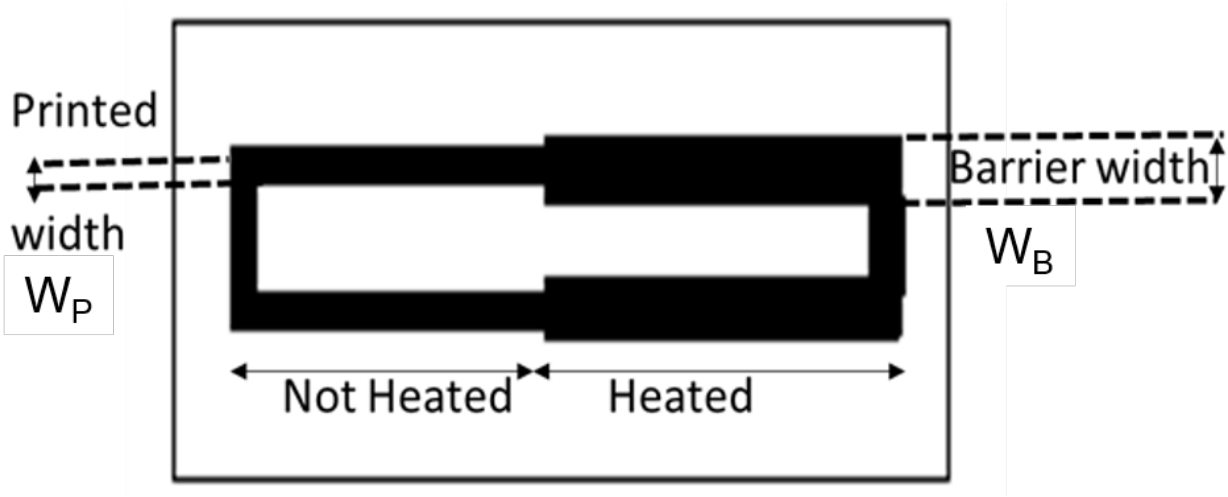

Figure 8. Representative sketch of the pattern printed to obtain barrier width. The left side represents the not heated side which shows the printed width. The right side shows the expanded printed width after heating which refers to as barrier width. The locations that are labeled represents the points that were used to take width measurements.

First, three hollow rectangular model microfluidic structures with outer dimensions of 5 $\times$ 1.5 cm were printed on filter paper with similar line widths. The paper with the printed design was then folded in half, and one half was placed on the hot plate while keeping the other half at a 90 ^{o} angle to the hot plate so that it would not contact the hot plate as depicted in Figure 9b.

Each shape was heated on the hot plate for 60 seconds at 140 ^{o} C, and allowed to cool for 30 minutes to room temperature. This process was repeated for each hollow rectangle and resulted in a hollow rectangle similar to the one shown in Figure 8.

The printed widths and barrier widths were measured on the front side of the paper using a vernier caliper. In order to obtain printed width, the non-heated side of Figure 9c was used. The measurements were taken approximately at 1/4, 1/2, and 3/4 along the line per specimen and the

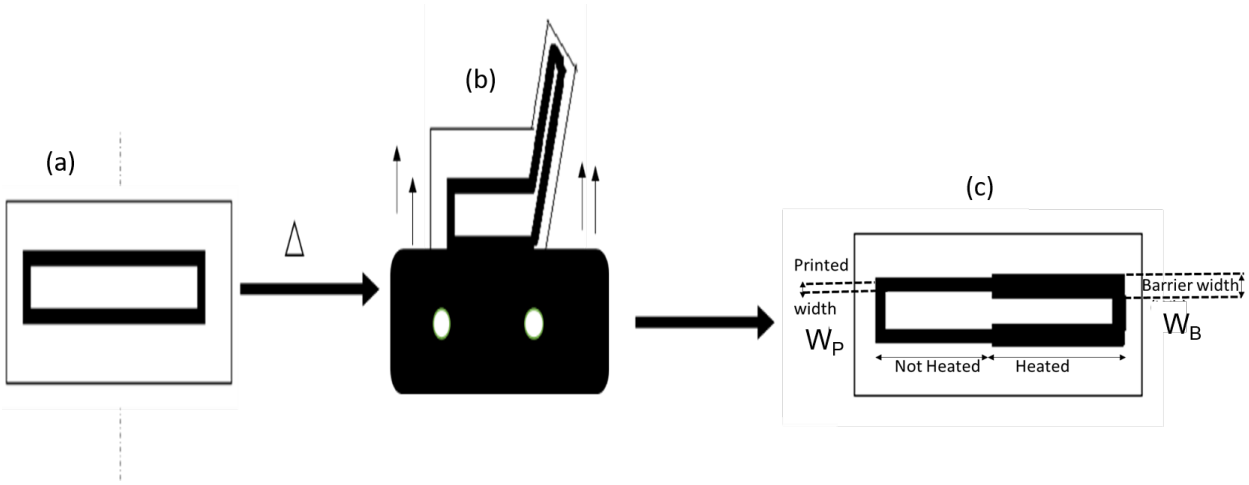

Figure 9. Schematic diagram of the process to make samples for measuring barrier width: (a). Printing the hollow rectangular shape, (b). Heating half of the printed shape. (c). Final shape with left half and right half representing the printed width and barrier width respectively.

average for the 3 measurements were calculated. Likewise, to get barrier width, 3 measurements were taken on the heated side of the rectangle at the marked sites and averaged. The same procedure was followed for the other 2 samples with similar printed widths. This procedure was repeated for four additional printed widths with outer dimensions of 5 cm x 1.5 cm. The average values of the measured widths, and resulting wax spreading distance L, are shown in Table 1.

Paper based analytical devices as μPADs were originally reported by Whitesides *et al.* in 2007. They reported similar trends in the relationship between the final barrier width and the original printed width at 150 ^{o}C when heated for 120 seconds,[34] and found the average spreading of L to be 0.27 mm.

According to Whitesides *et al.*[34] the linear relationship of barrier width and printed width can be represented as:

$$W_B = W_P + 2L \tag{2}$$

where W_B is the barrier width, W_P is the printed width, and L is the y-intercept and the distance

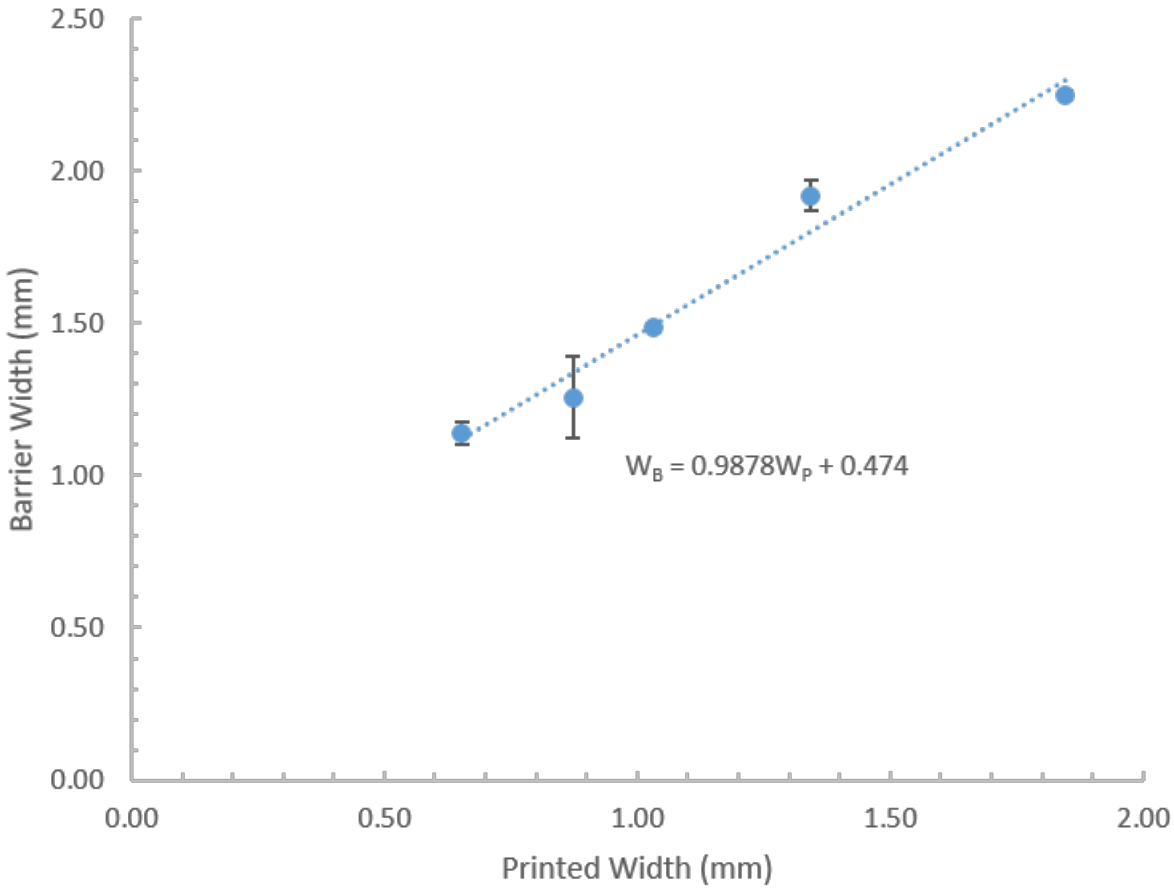

Figure 10. Quantitative assessment of the spreading of printed wax of the rectangular lines of the hollow shape. The x axis is the average printed widths (W_P), and corresponding y values are averages of measured barrier widths (W_B). The error bars represent 1 standard deviation in y axis.

Table 1. Average measured values for printed width, inner distance between printed lines and barrier width. The wax spreading distance L was calculated using (W_P) and (W_B).

Sample number	Average printed width W_P, mm	Average barrier width W_B, mm	Average space between printed lines, W_G, mm	Wax spreading distance,L, mm
1	1.85	2.25	11.31	0.20
2	1.34	1.92	12.31	0.29
3	1.03	1.49	12.93	0.23
4	0.87	1.26	13.25	0.19
5	0.65	1.14	13.69	0.24
Average			12.70	0.23

that wax spreads laterally.

In Figure 10 is shown the plot of W_P vs W_B with a linear fit of the data from the current study. The linear relationship between W_P and W_B was found to be:

$$W_B = 0.99W_P + 0.47 \tag{3}$$

yielding L to be 0.23 mm.

With the distance the wax spreads determined experimentally, the mathematical model describing the relationship between the printed channel width and the melted channel can be derived, and is shown in equation 4:

$$W_C = W_G - 2L \tag{4}$$

where W_C is the channel width, W_G is the printed channel width, and L is the y-intercept and the distance that wax spreads laterally. It was determined that L was 0.23 mm which is a good agreement of L value of 0.27 mm found by Whitesides *et al.*[34]

3.4 Validation prediction model for channel width creation

In order to test the utility of the model derived in section 3.3 in eqn 4, a validation set of experiments were conducted. The microfluidic structure with a T-shape (labeled as Tdesign) is shown in Figure 11. The Tdesign has a square end with 5 mm x 5 mm inner dimension which would work as the fluid reservoir. The total printed inner length of the long rectangular shape is a constant at 50 mm.

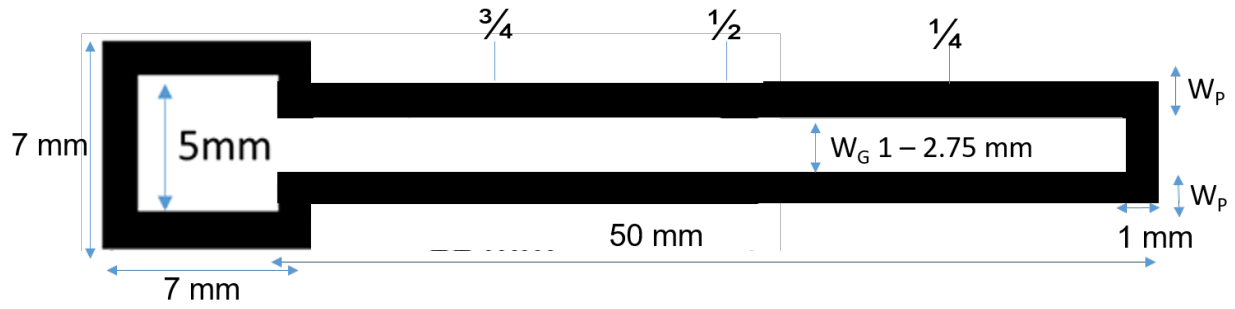

Figure 11. Schematic representation of the pattern with a T-shape (Tdesign) fabricated to study the effect of channel width on flow characteristics. The 5 mm x 5 mm square works as the sample reservoir. The long rectangular inner surface works as the flow channel and its width (W_G) was varied by changing the printed widths of the parallel lines (W_P).

The printed flow channel of width (W_G) was varied from 1 to 2.75 mm, by changing the printed widths (W_P) of the two parallel lines of the rectangular part of the shape. All other lines of the Tdesign were kept constant at 1 mm so that the length of the channel or the area of the fluid reservoir would not change. As shown in Table 2, three specimens of each of the five different samples with varying W_G's were printed to get a total of 15 trials.

Each Tdesign sample was heated on the hot plate at 140 ^oC for 60 seconds. As shown in Figure 11, the printed channels has a hydrophilic surface on the front and back of the paper. Thus, when a liquid sample is introduced, the liquid could leak or drip out of the paper. To avoid this leak, one side of the channel is sealed by attaching parafilm to the back of the Tdesign paper and

melting it by placing the other side of the paper on the hot plate for another 60 seconds at 140 ^{o}C.

The actual channel widths of these heated Tdesigns were measured approximately at 1/4th, 1/2nd and 3/4th along the long rectangular channel indicated in Figure 11. This data is tabulated in Table 2. For each printed width, 3 measurements were made to get a total of 18 measurements for all 6 samples.

As shown in Table 2, for each printed channel width, the theoretical channel width was calculated using the equation 4 and are listed in Table 2 in the second column. Columns 3-5 list measured channel widths of the rectangular channels at 1/4th, 1/2th and 3/4th positions after heating. The corresponding distance of liquid travelled is listed in the last column and will be described fully in Section 3.5.

In Figure 12, expected and actual channel widths were plotted against the printed widths. The X markers show the theoretical average channel widths for each printed channel width. The square markers represent the measured actual average channel width. Both data sets show that the channel width increases linearly when printed width is increased, and show that the predicted channel widths are very close to the actual final width.

Thus, based on this analysis, it can be concluded that the equation 4 is valid and the experimental procedure aligns with it. With the given experimental conditions, it would be possible to predict the channel width that is needed to achieve the desired channel width.

3.5 Finding the optimal channel width

In paper based microfluidic structures, the flow characteristics depend on many factors including the channel width, type of fibers, surface tension and viscosity of the liquids. The main drive for the liquids to flow on paper substrates is through capillary action, thus, the lower the channel width, the longer the liquid could flow. Thus, finding the narrowest functional channel width and understanding its flow characteristics are important in designing the μPAD.

After the microfluidic structures (Tdesign) described in Section 3.4 with various channel

Table 2. Printed channel width (W_P) , theoretically expected channel width after heating, the experimental channel widths after heating, and distance of liquid traveled for each channel width.

Printed channel width, mm	Expected channel width after heating, mm	Measured channel width, mm			Volume travelled distance, mm
		At 1/4th	At 1/2th	At 3/4th	
1.00	0.53	0.71	0.69	0.08	23.78
1.00	0.53	0.77	1.08	1.03	30.51
1.00	0.53	0.72	0.83	0.68	28.23
1.25	0.78	1.17	0.88	0.77	36.61
1.25	0.78	1.27	0.98	1.04	24.01
1.25	0.78	1.04	1.16	1.19	31.24
1.50	1.03	1.26	1.07	1.19	33.89
1.50	1.03	1.25	1.15	1.16	32.76
1.50	1.03	1.33	1.66	1.27	32.06
1.75	1.28	1.66	1.57	1.71	24.57
1.75	1.28	1.67	1.68	1.68	28.2
1.75	1.28	1.67	1.77	1.84	29.38
2.25	1.78	2.08	2.25	2.19	11.04
2.25	1.78	2.28	2.21	2.13	26.63
2.25	1.78	2.28	2.32	2.32	23.02
2.75	2.28	2.36	2.26	2.31	17.77
2.75	2.28	2.35	2.44	2.4	22.37
2.75	2.28	2.6	2.71	2.74	18.61

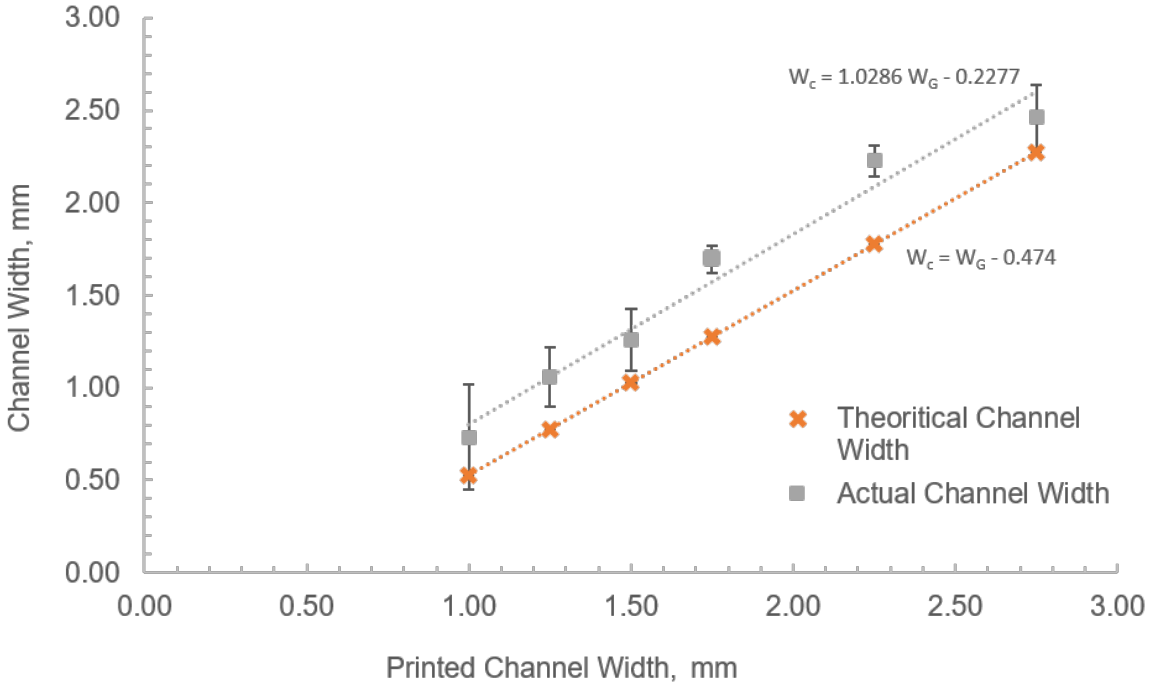

Figure 12. Expected and actual average channel widths vs printed channel width.

widths were constructed and measured, they were tested for liquid flow characteristics as follows. A food coloring solution was used to identify the location of the liquid, which was prepared by diluting 1 mL of red food coloring with of deionized water in a 10 mL volumetric flask. First, additional Tdesign structures were used to optimize the volume of liquid needed to add to the sample reservoir to get a better performance. When a liquid sample is added to the sample zone (square reservoir), it was found that if less than 5 mL of solution was added, it was not enough volume to flow all the way to the end of the channel. If the volume was more than 5 mL, then the liquid overflowed the edge of the reservoir before flowing out to the channel. Therefore it was determined that a volume of 5 mL of solution would be used to determine the flow characteristics for the current Tdesign.

Then, the distance liquid travelled after 10 seconds of initial solution added was determined

by the video camera procedure described in Section 2.2.6. When video playback was used to monitor the liquid flow distances, it was noted that the liquid in the Tdesign with the smallest channel width stopped flowing after 10 seconds. The liquid in some Tdesigns kept moving even after 30 seconds. In order to include the distances traveled from each channel width, the flow distance travelled at 10 seconds was chosen and are listed in last column of Table 2.

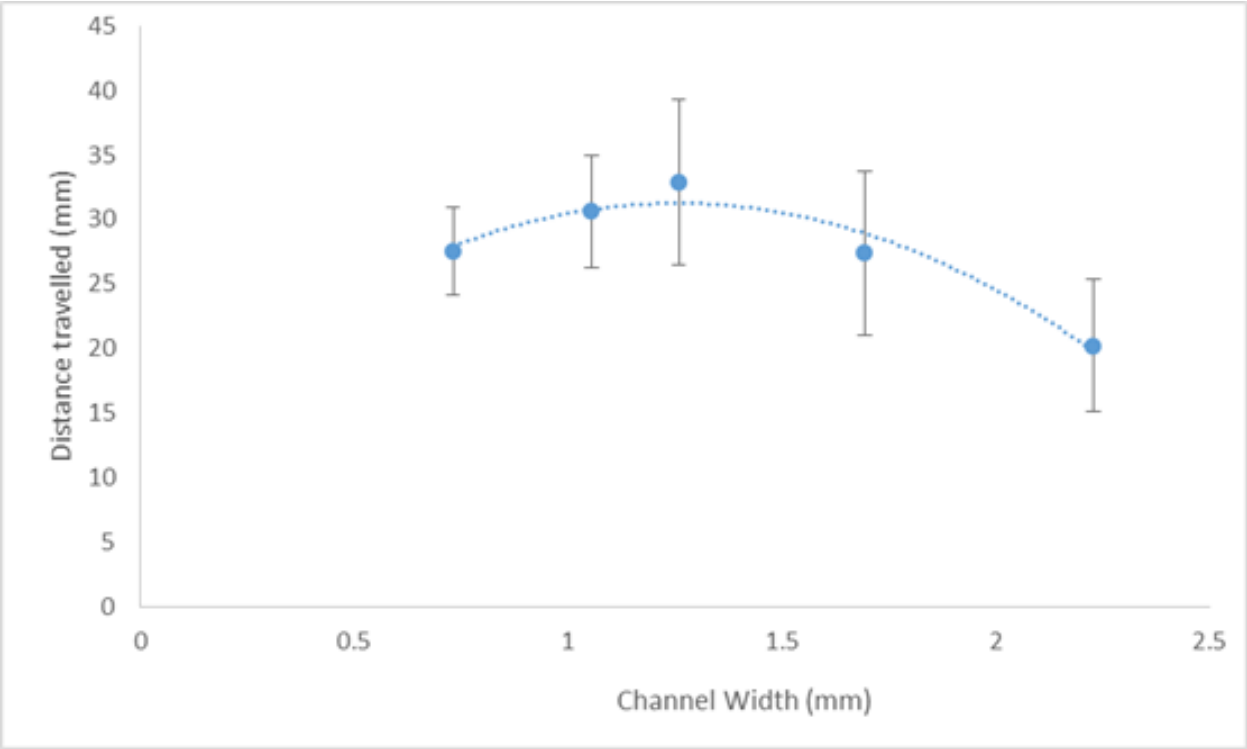

Figure 13. Distance of food coloring traveled for each channel width at 10 seconds. At narrower channel widths, the distance traveled was lower, and gets maximized before lowering down at higher channel widths.

In Figure 13 is shown the liquid travel distance as a function of channel width. The graph shows a parabolic shape with a maximum between 1 – 1.5 mm channel width. In Figure 13, the flow profile follows the typical Washburn behavior up to the channel width corresponding to the maximum travel distance. According to the Washburn model, the distance traveled by the fluid

front at constant time is proportional to the square root of average pore size and surface tension which can be described by the following equation:

$$x = \sqrt{\frac{\gamma}{\mu}\frac{cos\theta}{2}r_c t} \tag{5}$$

where x is distance travelled, γ is the surface tension of the liquid, θ is the contact angle, μ is the viscosity of the fluid, r_c is the average pore radius of the pores within fibers in paper, and t is the time.

In the present experiment, the viscosity of the fluid and the time the fluid travelled were kept constant. The contact angle could vary across the channel at hydrophobic boundaries and inner hydrophilic fibers. In the hydrophilic areas, the contact angle between water and Whatman-paper-fiber surface (22^o)[77] is lower than water and paraffin wax (112^o - 130^o)[78] providing a higher value in Cos θ. Thus, the adhesive strength between water and hydrophilic fibers is higher than between water and hydrophobic wax. Thus, more of the hydrophilic area, the higher distances the liquid flows. At smaller widths less than the maximum, the surface tension at the hydrophobic boundaries made by wax layers is more significant than in the wider channels. Further, at lower channel widths, the percentage of hydrophobic area is significantly higher. Thus, the flow of the liquid at channel boundaries was slower which caused the liquid to flow lower distances.

Further, the percentage of porosity in the microfluidic flow channel is lower at smaller widths due to clogging of pores at the hydrophobic boundaries by wax. Due to these differences, at smaller widths, flow speed would be slower and the distance that the fluid travels at a constant time is lower. After the channel width that corresponds to the maximum distance, the effects of these phenomena are overpowered by the Darcy Law which defines the ability of a liquid to flow through a porous media.[79] It's based on the flow of a liquid as a function of pressure drop along the channel and at the cross section. In the current Tdesign microfluidic paper, the area of the fluid flow from reservoir drops dramatically at the entrance of the flow channel increasing the

fluid pressure.

At high pressure, the liquid flow rate is higher. However, when the width of the channel increases, the pressure difference is reduced, which in turn, reduces the liquid flow speed. Accordingly, above 1.5 mm channel width, the pressure is decreased at the cross section where the liquid in the main square reservoir enters the rectangular channel, and as a result, flow rate is decreased. In Figure 13, this phenomena was clearly seen after approximately 1.3 mm channel width.

The channel width that allows for the most distance is found by fitting the travel distance vs channel width with a polynomial and finding the maximum using calculus. The best fit function is:

$$L = -12.118W_C^2 + 30.455W_C + 12.115 \tag{6}$$

where L is the distance liquid travelled, and W_C is the channel width. According to the equation, the maximum distance would be at W_C = 1.26 mm.

In μPADs, the liquid is expected to travel all the way to the end of the channel, where the detection zone with appropriate reagents are located. Thus, in the design, the channel width where it allowed the liquid to the flow maximum distance is 1.3 mm.

3.6 Preparation of μPADs for analysis of water hardness

As shown in Figure 14, the design of the μPADs consists of a sample reservoir in the middle with 10 hydrophilic channels attached to it. The hydrophilic channels have 10 inner circles which are reaction zones with various concentrations of EDTA and ten outer reservoirs where constant amounts of metal ion indicators are located. In order to determine the total hardness and the individual concentrations of calcium and magnesium ions, two separate titration reactions needed to be carried out at pH 10 for total water hardness and pH 13 for calcium. Magnesium concentration was determined by the difference between the two concentrations.

For the determination of total water hardness, the pH of the μPADs needed to be maintained at 10 using the CAPS buffer. The ten reaction reservoirs contained EDTA and EBT was selected to be at the detection zone as metal ion indicator.

For determination of individual calcium concentration, another titration was carried out at pH 13 using KOH. In the presence of KOH, magnesium ions precipitate as magnesium hydroxide, while calcium ions do not. Thus, at pH 13, only the calcium ions are available to react with EDTA and excess calcium ions with metal ion indicator Calcon.

The following sections describe the approaches that were taken to develop the desired μPADs for total water hardness at pH 10 and direct measurement of calcium concentration at pH 13 and indirectly, the magnesium concentration.

3.6.1 Overall design features of μPADs

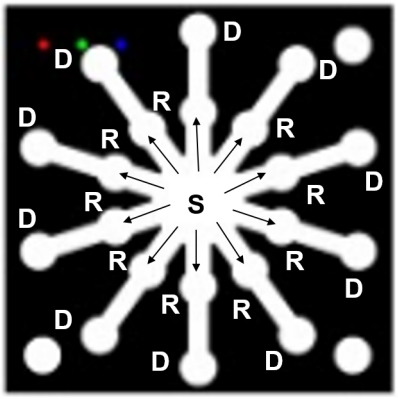

Figure 14. Diagram of the designed μPAD for water analysis. The ten detection zones where the metal-indicator reacts with metal ions are labeled as D, ten reactions zones where EDTA reacts with metal ions are labelled as R, the inner circle where the sample solution is added is labeled as S. The arrows shows the directions where all the analytes flow on the μPAD.

In Figure 14 is shown the general design of the μPAD that was developed. The diameter of the round microfluidic structure was 50 mm. It has three main areas. The area labeled **S** is the area where the sample is applied. The arrows show the directions that the sample travels. The samples travel via the channels to the inner circles, labelled as **R**, where different, sequential concentrations of EDTA are located. The cations react with EDTA creating a cation-ligand complex. In the channels where the amount of cation is greater than the EDTA, the excess free cations flow toward the 3rd zone labelled as **D**. The indicator complexes the free, excess cations, which results in a color change

With this design, the concentration of the analyte can be determined by the EDTA concentration of the very first changed colored circle adjacent to the last unchanged circle.

3.6.2 Selection of pH 10 buffer

At pH values lower than 10, EDTA does not react in a 1:1 ratio with Mg^{2+} ions, thus free ions could travel to the detection zone yielding false positive results. Three different buffers were explored to maintain the pH of 10 on the μPAD, which include sodium carbonate/sodium bicarbonate, sodium tetraborate, and N-Cyclohexyl-3-aminopropanesulfonic acid (CAPS) buffer systems.

3.6.3 Evaluation of sodium carbonate /sodium bicarbonate buffer system

Initially sodium carbonate/sodium bicarbonate that was formulated as a pH 10 buffer was used on the μPAD for the total water hardness titration. To test its usability as a μPAD buffer, the buffer and the μPAD was prepared as described in section 2.2.4. It was titrated with 30 mM of Ca^{2+}, 30 mM of Mg^{2+} and 30 mM of equal concentrations of Ca^{2+} and Mg^{2+} solutions.

When 60 μL of 30 mM Ca^{2+} solution was added on to the μPAD, the expected color change was not observed. As shown in Figure 15 (a), the only color change that was observed was in the detection right next to 0 mM EDTA.

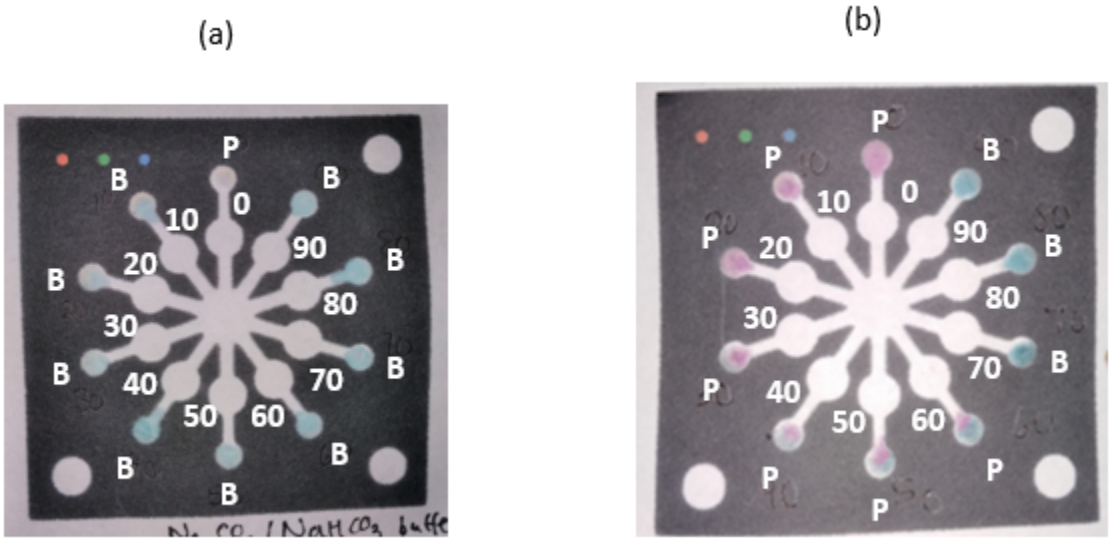

Figure 15. Titration with sodium bicarbonate-sodium carbonate buffer with EDTA in reaction zones and EBT in detection zones. (a) titration of the calcium (b) titration of magnesium. The EDTA solutions are in reaction zones, and their concentrations are labelled. The B (Blue) and P(Purple) corresponds to the color observed after adding respective analyte to the μ PADs.

A blue to purple color change was observed when 60 μL of the 30 mM Mg^{2+} solution was added onto the prepared μPADs. However the expected color change is at 0 - 20 mM of purple and all other detection zones to be blue. However, as shown in Figure 15, the color change was observed beyond the expected zones where a blue to purple color is seen in detection zones next to 0 - 60 mM. According to this observation, the end point of this solution is 70 mM which is too high. Therefore the root cause analysis for the false negative results for Ca^{2+} and false positive results for Mg^{2+} was performed.

3.6.4 Root cause analysis for false results with sodium carbonate/sodium bi-carbonate buffer system

In order to discover the reason for the lack of color change with calcium using this buffer, aqueous reactions were carried out using a black spot plate. When a titration was carried out in

solution, it was discovered that the sodium bicarbonate / sodium carbonate buffer produces a precipitate with the calcium cation but not with the magnesium cations. The solubility product equilibrium constant (K_{sp}) is used for describing the dissociation and subsequent solubility of ionic compounds. Analysis of the K_{sp} suggest that magnesium is more soluble than calcium at pH 10 in the carbonate form. The K_{sp} for calcium carbonate is 2.8x 10^{-9}, and the K_{sp} value for magnesium carbonate is 3.5x10^{-8}.[80] Thus the calcium would precipitate in the presence of this buffer making it not be suitable for constructing μPADs. In the μPAD, the reaction channel marked as 0 mM does not have any EDTA in its reaction zone. Thus, any cations that go through this channel are not complexed and will always form a complex with the indicator, EBT, resulting a color change from blue to purple.

3.6.5 Evaluation of sodium tetraborate buffer system

The second buffer that was tested for pH 10 on the μPAD was sodium tetraborate where pH 10 was achieved with a mixture of sodium tetraborate and sodium hydroxide. The buffer solutions and the related μPAD as described in section 2.2.4, was tested for its suitability at pH 10 was tested.

First, for testing the capability of μPAD, it was titrated with three different standard solutions; 30 mM of Ca^{2+}, 30 mM of Mg^{2+} and a mixture of 30 mM of equal concentrations of Ca^{2+} and Mg^{2+} solutions. In Figure 16 (a) is shown the titration of 30 mM calcium ion solution with the tetraborate buffer. In Figure 16 (a), the color change of purple to pink was not observed. In fact, a light pink color was observed in the detection zones next to 40 - 90 mM, while 10 - 30 mM zones remained blue. The only purple color change that was observed is at 0 mM zone.

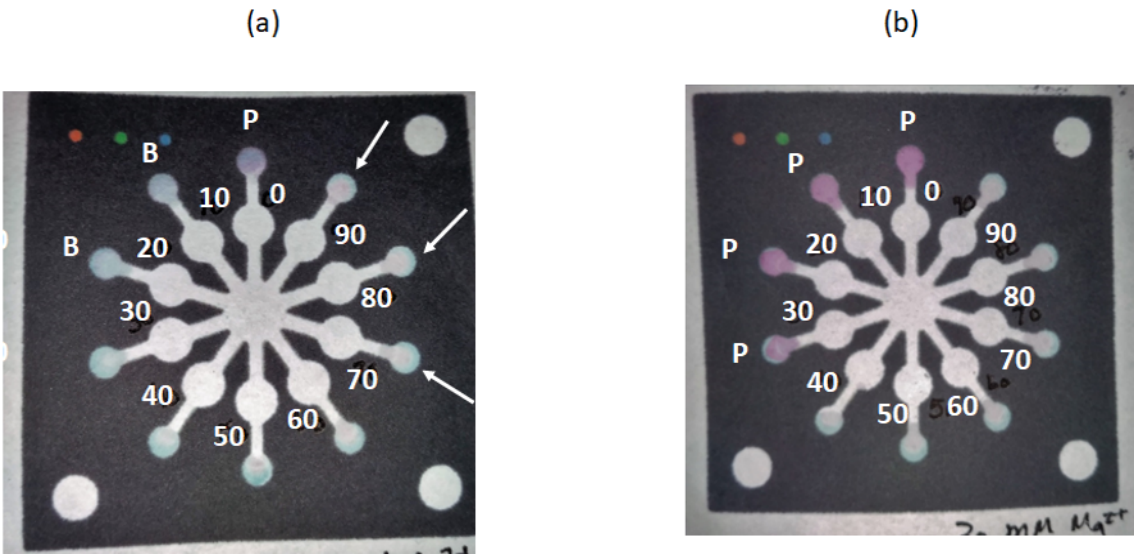

Figure 16. Titration with sodium tetraborate buffer at pH 10 using EBT as the indicator. (a) Titration of the 30 mM calcium and (b) titration of 30 mM magnesium. The EDTA solutions were added on to the 10 reaction zones, and their concentrations were labelled from 0 - 90 mM. The labels B and P correspond to the color observed at detection zones after adding samples to the μPADs.

In Figure 16(b) is shown the μPAD after 30 mM magnesium ion solution was added. A change of color from blue to pink was observed in the detection zones 0, 10 and 20 mM. As shown by the arrows in Figure 16 (a), the calcium solution yielded slightly pink areas randomly, revealing that sodium tetraborate was not suitable for use as a pH 10 buffer in the μPAD. Thus, suitability of another buffer solution, N-Cyclohexyl-3-aminopropanesulfonic acid (CAPS) was also tested.

3.6.6 Evaluation of N-Cyclohexyl-3-aminopropanesulfonic acid (CAPS) buffer system

The last buffer system that was tested is N-Cyclohexyl-3-aminopropanesulfonic acid (CAPS). To test if it is suitable to be used at pH 10, the μPADs with the buffer was prepared as in section 17.

First, three different μPADs were titrated with three different standard solutions; 30 mM of Ca^{2+}, 30 mM of Mg^{2+} and 30 mM of equal concentrations of Ca^{2+} and Mg^{2+} solutions.

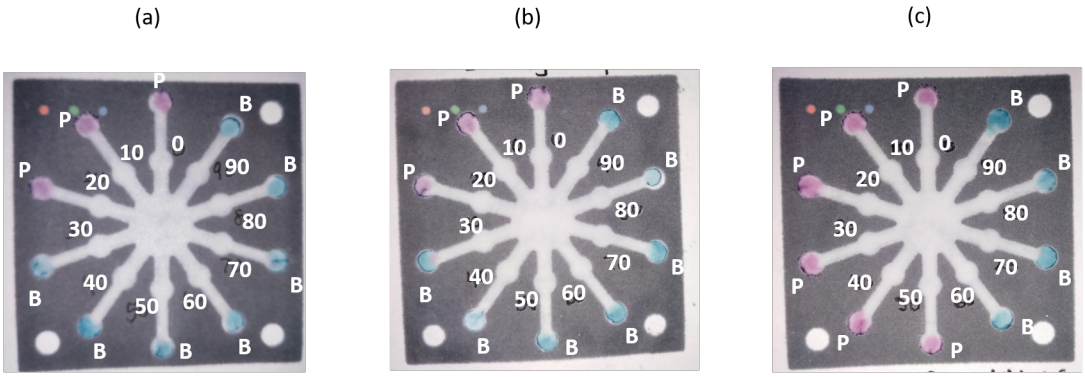

Figure 17. The titrations of magnesium and calcium at pH 10 using CAPS buffer and EBT indicator: (a) 30 mM Ca^{2+} titration (b) 30 mM Mg^{2+} titration and (c) mixture of 30 mM Ca^{2+} and 30 mM Mg^{2+} titration

When a 30 mM Ca^{2+} solution is titrated using the μPAD, it is expected to have a color change only at the detection zones adjacent to 0, 10 and 20 mM EDTA zones. As shown in Figure 17 a, the titration of 30 mM Ca^{2+} produces a color change from blue to purple in the detection zones right next to 0 - 20 mM EDTA. This confirms the concentration of calcium ions of 30 mM, and implies that the μPAD is working correctly.

In Figure 17 b, the titration of 30 mM Mg^{2+}, solution also produced similar results indicating that end point of 30 mM. In the mixture of 30 mM Ca^{2+} and 30 mM Mg^{2+} ions solution, the total concentration is 60 mM, thus, color changes from detection zones 0 - 50 mM was expected. As shown in Figure 17 c, the color change of blue to purple is observed in the detection zones right next to 0 – 50 mM, which implies that the end point was 60 mM. Thus, CAPS would be the satisfactory buffer to use in making the μPAD for titrating for total water hardness.

3.6.7 Testing for Ca^{2+} concentration in the presence of Mg^{2+}

EDTA is considered to be a highly unselective chelating agent due to its ability make complexes with doubly, triply or even quadruple charged cations.[1] Thus, in a medium where more than one complex forming cations are present, several procedures can be used to get selective re-

action with a metal cation of choice. Such procedures include the use of a masking or demasking agent, pH control and the use of selective metal indicators. In highly alkaline solutions, when the hydroxyl ion concentration is increased, metal hydroxides with low solubility form precipitates. At pH 13, in a mixture of Ca^{2+} and Mg^{2+} ions both react with hydroxide to form $Ca(OH)_2$ and $Mg(OH)_2$, respectively. The solubility of $Mg(OH)_2$ is much lower than for $Ca(OH)_2$. In the present study, in order to determine the calcium ion concentration in the presence of magnesium cations, magnesium cations were precipitated by adding KOH to the μPADs.

As a solid $Mg(OH)_2$ does not migrate with the solvent in the flow channels, it does not react with EDTA and consequently it does not form a complex with the indicator. So any resulting color change is indicative of only the presence of Ca^{2+} ions.

At pH 13, Eriochrome Black T (abbreviated as $H_2In_A^-$) exists in its third ionization state (In_A^{3-}) and has a pink color in its free form. Its complex with calcium ion is also pink in color,[74] thus, it is not suitable as a metal ion indicator at pH 13. Calcon (abbreviated as $H_2In_B^-$), at pH 13, exists as HIn_B^-. As shown in Figure 18, at pH 13, the uncomplexed free calcon which exist as HIn_B^{2-} is blue, and the color changes sharply from blue to pink-red when complexing with calcium ions.[74] Thus, Calcon was selected to be used as the metal ion indicator for complexing with Ca^{2+} ions at pH 13.

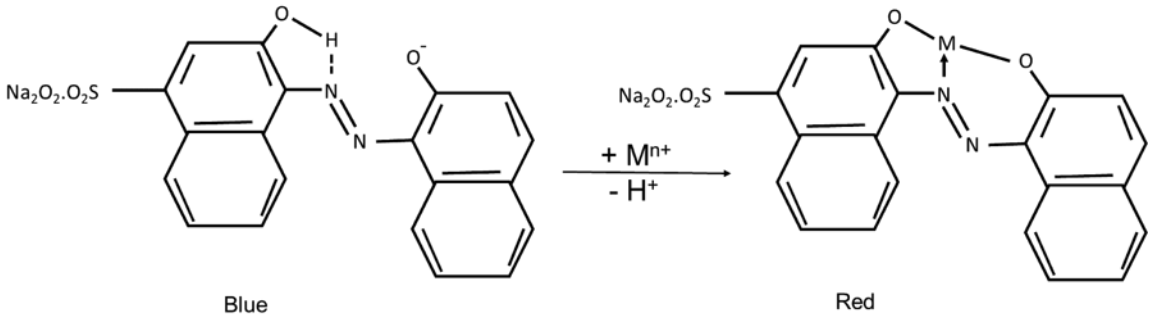

Figure 18. Schematic representation of the color reactions of metal ion indicator Calcon with metal ions M^{n+}.

3.6.8 Standardization of μPADs

In order to check the accuracy of the μPADs made for pH 13, they were titrated with three standard solutions of 30 mM Ca^{2+}, 30 mM Mg^{2+}, and a mixture of 30 mM Ca^{2+} and 30 mM Mg^{2+} solutions as follows.

Thus, initially, 60 μL of 30 mM Ca^{2+} solution was added to the sample zone of the μPAD, and it was determined that this volume was not enough to reach the detection zone. After the trial and error method, it was found that, 80 μL of sample solutions was needed for titrating samples using the μPADs.

The three standard solutions were titrated and the results are shown in Figure 19. The color of the detection zones changed from blue to purple at detection zones that are adjacent to reaction zones containing 0, 10 and 20 mM of EDTA. The end point is determined by the blue colored detection zone with the adjacent lowest concentration of EDTA in reaction zone, which corresponds to 30 mM. This result shows that the μPAD successfully titrated the standard Ca^{2+} solution and provided the accurate concentration determination.

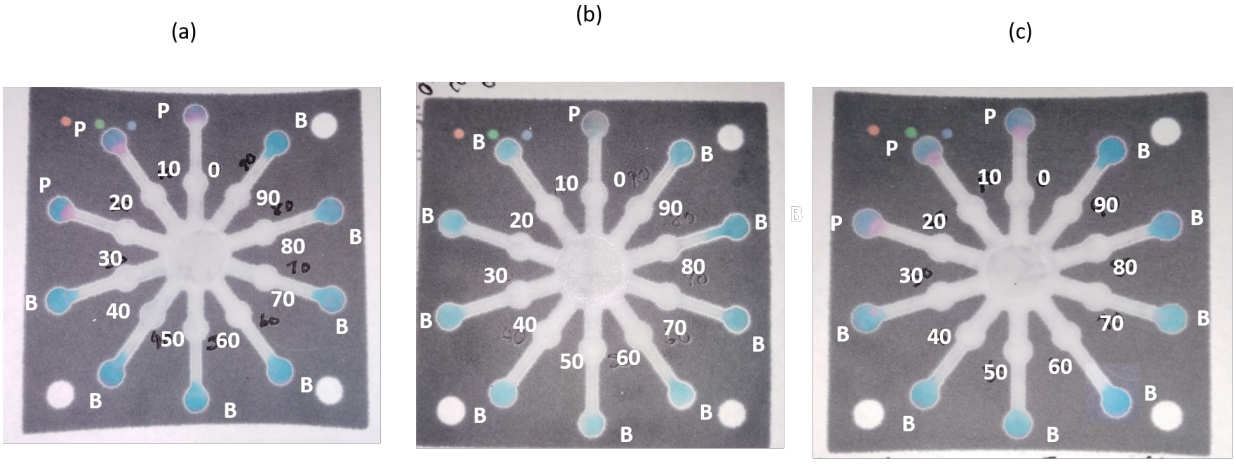

Figure 19. The titrations of magnesium and calcium at pH 13 using KOH and calcon indicator: (a) 30 mM Ca^{2+} titration (b) 30 mM Mg^{2+}, titration and (c) mixture of 30 mM Ca^{2+} and 30 mM Mg^{2+} titration.

When Mg^{2+} solution was added to the μPAD at pH 13, as expected, there was no color change at any of the detection zones except the zone corresponding to 0 mM EDTA. It was found that the nano pure water that was used for making the reagents are not very pure, and could have some Ca^{2+} coming from the water source making a slight pink color change at 0 mM zone. However, with no color change at the 10 and 20 mM detection zones, it was concluded that the μPAD was working correctly and Mg^{2+} precipitated to form $Mg(OH)_2$ at the center sample zone where pH is adjusted to 13 with KOH.

Last, a new μPAD was titrated using 80 μL of standard solution of the 30 mM Ca^{2+} and 30 mM Mg^{2+} mixed solution. As shown in Figure 19c, the color change was seen only at 0, 10 and 20 mM detection zones. Thus, the μPAD was working correctly and capable of separating a mixture of Ca^{2+} and Mg^{2+} ion solutions.

3.7 Collection of unknown water samples to be analysed by μPADs

In order to evaluate the effectiveness and applicability of the μPADs, water were collected samples from various sources including creeks, rivers, wells and commercially available water bottles. To get representative samples, river, creek and lake water was collected far away from the bank. Samples were collected and stored in glass jars. The water sources and the location where they were collected are listed in the Table 3.

Table 3. The sources of unknown water sample and their locations.

Water source	Location	GPS collection coordinates
Gerber	Bottled water	N/A
Scott Creek	Sylva, NC	35^0 24′ 8.48″ N 83^0 6′ 40.60″ W
South River	Sylva, NC	35^0 20′ 27.79″ N 83^0 12′ 48.78″ W
Laurel Oaks Apatments	Cullowhee, NC	35^0 18′ 9.29″ N 83^0 11′ 52.44″ W
Well Water	Sylva, NC	35^0 20′ 13.79″ N 83^0 15′ 45.62″ W
Lake Dillisboro	Dillisboro, NC	35^0 22′ 0.36″ N 83^0 14′ 59.53″ W

Also a commercially available Gerber brand water which is advertised as mineral water for infants and children was also purchased from the store. The water samples were used for testing without any further treatment. The commercially available Gerber Pure Purified water sample was obtained from Walmart store which comes in a 1- gallon container. This water is enriched with minerals magnesium sulfate, calcium chloride and potassium bicarbonate. Gerber purified water is manufactured to mix with infant formula to provide the essential minerals and nutrients to toddlers and to enhance the taste. A sample of water was collected from Lake Dillsboro, closer to the Best Western hotel to which is close to a local cement plant. It was hypothesized that the cement plant would excrete the calcium rich waste products into the water. The water sample collected from a stream that is running along the Scott Creek in Sylva, NC. The location in which the sample was collected was next to a place where a lumber mill is located. Thus, it was hypothesized that some of the water runoff might affect waterways adjacent to the mill. The South River

waterway sampling location is located about 10 miles away from Western Carolina University, in front of multiple residential houses. Laurel Oaks apartments sampling location is an apartment complex located a mile away from WCU. The well water sample was collected from a house in Sylva. Since the water is from a well in a rural area, it has not been tested for its hardness previously. The samples were taken from a tap after directly pumping to the source.

3.8 Analysis of unknown water samples

In order to be used with unknown samples, two sets of μPADs with a microfluidic structure given as in Figure 14 were made and prepared to detect within 10 mM – 90 mM range at pH 10 and 13.

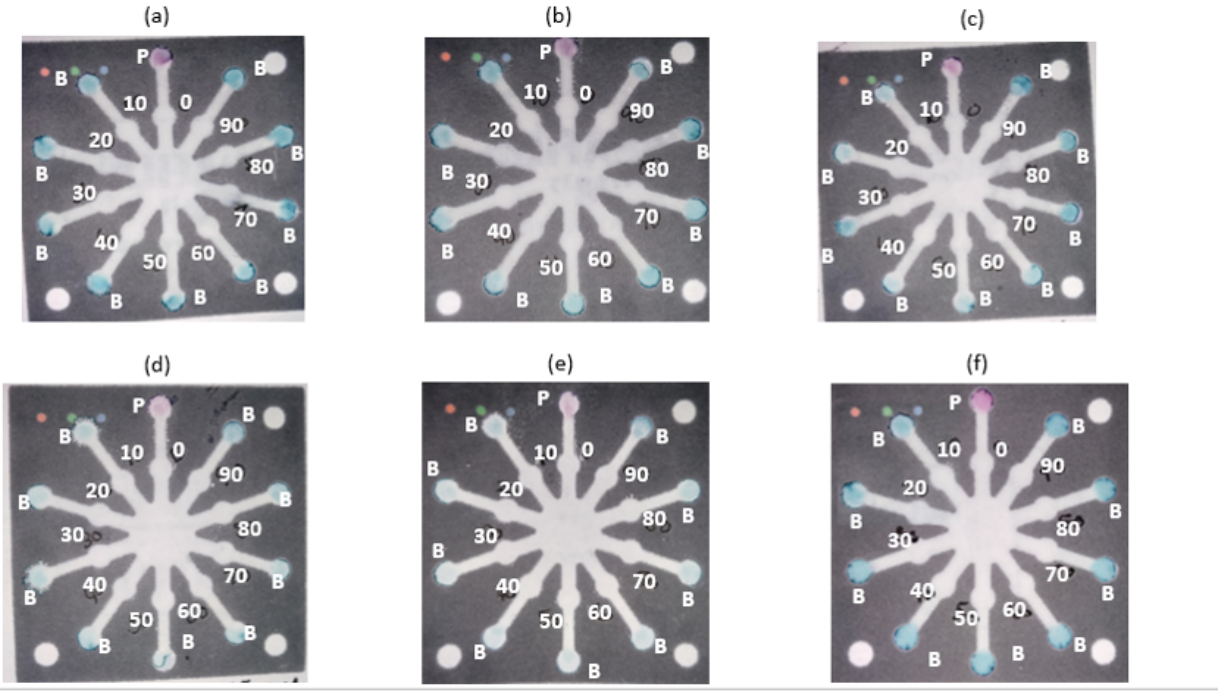

Figure 20. Titrated μPADs with 0 - 90 mM detection range. CAPS was used as buffer for pH 10 titration and EBT was used as the indicator. The EDTA concentrations from 0 - 90 mM are the in reaction zones. Titrated with (a) Scott Creek (b) South River (c) Well water, (d) Lake Dillisboro, (e) Laurel Oaks and (f) Gerber Pure water.

Then 80 μL of each of the unknown samples were added using new μPADs. Pictures of the resulting μPADs are shown in Figure 20. The titrated water samples include (a) Scott Creek (b) South River (c) Well water, (d) Lake Dillisboro, (e) Laurel Oaks and (f) Gerber Pure water, and the color changed detection zones are marked as P for changing to purple and B for original blue color. All samples changed colors at detection zone corresponding to 0 EDTA, however, all other 9 detection zones remained its uncomplexed-EBT color blue. According to this results, it was concluded that the total hardness of the unknown water samples could be between 0 - 9 mM.

3.9 Testing the unknown water samples with μPADs with 0 - 9 mM detection zones

As as described in section 2.2.1, new μPADs with EDTA concentrations ranging from 0 to 9 mM were prepared. As shown in Table 4, when Gerber water was titrated at pH 10, the detection zones adjacent to 0 - 7 mM EDTA sample zones changed color from blue to purple, while detection zones 8 and 9 mM did not. Thus, the total hardness of Gerber water is determined to be 8 mM which implies that the total concentration of the Ca^{2+} and Mg^{2+} ions in this water was 8 mM. Among all the samples evaluated, Gerber water had the highest level of water hardness which was expected since the water was enriched with both calcium and magnesium.

In order to check and determine individual concentration of Ca^{2+} ions of Gerber water, μPADs made for pH 13, was titrated with Gerber water. As shown in Table 4, the detection zones adjacent to 0 - 4 mM EDTA sample zones changed color from blue to purple, while detection zones 5 and 9 mM did not. Thus, the Ca^{2+} ion concentration in Gerber water is determined to be 5 mM. These two titrated results revealed that the Ca^{2+} and Mg^{2+} ion concentrations in Gerber water was 5 mM and 3 mM, respectively.

Table 4. Magnesium and calcium ion concentrations of the unknown water samples determined by μPADs and ICP-OES.

Water Source	μPAD pH 10	μPAD pH 13	μPAD Total Hardness mM	μPAD [Ca] mM	ICP [Ca]mM	μPAD [Mg] mM	ICP [Mg] mM
Gerber	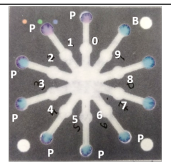	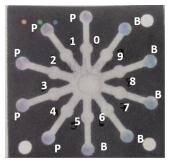	8±1	5±1	4.0±0.45	3±1	5.0±0.45
Lake Dillisboro	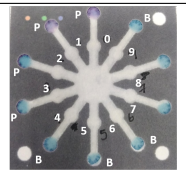	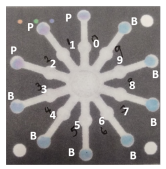	5±1	3±1	0.8±0.45	2±1	0.7±0.45
Scott Creek	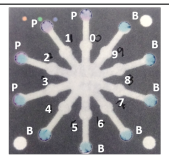	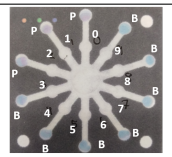	4±1	3±1	1.1±0.45	1±1	1.2±0.45
South River	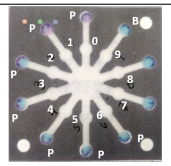	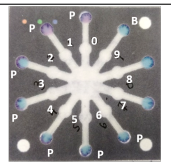	2 ±1	2±1	0.7±0.45	0±1	0.5±0.45
Laurel Oaks	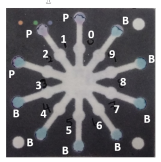	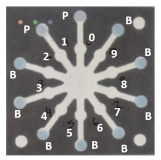	3±1	2±1	1.1±0.45	1±1	0.3±0.45
Well water	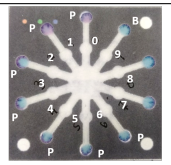	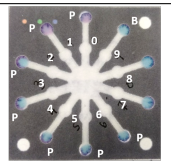	4±1	2±1	2.4±0.45	2±1	1.5±0.45

Next, Lake Dillisboro water was titrated with μPADs at pH 10. As shown in Table 4, the detection zones adjacent to 0 - 4 mM EDTA sample zones changed color from blue to purple, while detection zones 5 and 9 mM did not, indicating the total hardness of Lake Dillisboro water is 5 mM. Then the μPADs made for pH 13 was titrated. As shown in Table 4, the detection zones adjacent to 0 - 2 mM EDTA sample zones changed color from blue to purple, while detection zones 3 and 9 did not. Thus, the Ca^{2+} ion concentration in Lake Dillisboro water is determined to be 3 mM.

When the Scott Creek water was titrated at pH 10 using the μPADs, as shown in Table 4, the detection zones adjacent to 0 - 3 mM EDTA sample zones changed color from blue to purple, while detection zones 4 and 9 mM did not. Thus, the total concentration of the Ca^{2+} and Mg^{2+} ions in this water was 4 mM.

To determine concentration of Ca^{2+} ions of Scott Creek water at pH 13, the μPADs were titrated with Scott Creek water. As shown in Table 4, the detection zones adjacent to 0 - 2 mM EDTA sample zones changed color from blue to purple, while detection zones 3 and 9 mM did not. Thus, the Ca^{2+} ion concentration in Scott Creek water is determined to be 3 mM.

Next, South River water was titrated at pH 10 using the μPADs and as shown in Table 4, the detection zones adjacent to 0 - 1 mM EDTA sample zones changed color from blue to purple, while detection zones 2 and 9 did not. Thus, the total concentration of the Ca^{2+} and Mg^{2+} ions in this water is 2 mM.

When South River water was titrated at pH 13, as shown in Table 4, the detection zones adjacent to 0 - 1 mM EDTA sample zones changed color from blue to purple, while detection zones 2 and 9 mM did not. Thus, the Ca^{2+} ion concentration in South River water is determined to be 2 mM. The calcium levels at pH 13 was 1 - 2 mM which indicates that there is < 1 mM of magnesium metal present in this water sample. Hence, the results indicate that the calcium levels are higher than magnesium levels in the South River water.

As shown in Table 4, in titrated μPADs for Laurel Oaks apartments water, the detection zones

adjacent to 0 - 2 mM EDTA sample zones changed color from blue to purple, while detection zones 3 and 9 did not. Thus, the total concentration of the Ca^{2+} and Mg^{2+} ions in this water was 3 mM.

When Laurel Oaks apartments water was titrated at pH 13, the detection zones adjacent to 0 - 1 mM EDTA sample zones changed color from blue to purple, while detection zones 2 and 9 mM did not, indicating that the Ca^{2+} ion concentration in Laurel Oaks apartments water is determined to be 2 mM. Based on the total water hardness and the calcium concentration, the magnesium concentration is 1 mM. Further, it suggests that the calcium levels present in the water is significantly higher than the magnesium.

As shown in Table 4, after testing well water at pH 10, the detection zones adjacent to 0 - 3 mM EDTA sample zones changed color from blue to purple, while detection zones 4 and 9 did not. Thus, the total concentration of the Ca^{2+} and Mg^{2+} ions in this water was 4 mM.

When well water was titrated at pH 13, the detection zones adjacent to 0 - 1 mM EDTA sample zones changed color from blue to purple, while detection zones 2 and 9 mM did not. Thus, the Ca^{2+} ion concentration in well water is determined to be 2 mM which makes the Mg^{2+} ion concentration to be 2 mM.

3.10 Validation of concentrations of Ca^{2+} and Mg^{2+} ions in unknown samples by Inductively Coupled Plasma Atomic Emission Spectroscopy (ICP-OES)

The total concentrations of Ca^{2+} and Mg^{2+} in each unknown water samples were validated externally with Inductively Coupled Plasma Optical Emission spectroscopy (ICP-OES). Table 4 shows a comparison of Ca^{2+} and Mg^{2+} ion concentrations of unknown samples measured by ICP-OES and the μPADs. According to the results, Ca^{2+} concentrations of unknown water samples determined by μPAD and ICP-OES were a close match with some samples while some were different. The differences in values could probably be due to some interferences with other metal ions which would be discussed in section 3.12. Overall, these results show that the developed

μPADs provide a close Ca^{2+} and Mg^{2+} ion concentrations in unknown samples.

3.11 Analysis of the effect of interferences on the accuracy of μPAD readings

The primary sources that are contributing to hardness in water are dissolved polyvalent metallic ions, sedimentary rocks and runoff from soils, etc. These polyvalent metallic ions in water are predominantly magnesium and calcium ions, however, other cations including aluminum, barium, manganese, zinc, strontium, iron etc. could also be present in water. In order to check whether these ions potentially interfere with the determination of Ca^{2+} and Mg^{2+} ions concentrations, five different ions were tested. The ions that were tested are iron, copper, nickel, manganese, and aluminum. These ions were titrated using the μPAD made with CAPS buffer at pH 10 with the EBT indicator and various concentrations of EDTA in reaction zones.

EDTA usually reacts with polyvalent metal cations on a 1:1 molar ratio. The equilibrium constant of a reaction between metal ion and a ligand is defined as the formation constant. For example, when a metal ion M^{n+} reacts with EDTA ligand Y^{4-}, formation constant K_f can be defined as follows.[73]

$$\mathrm{M^{n+}} + \mathrm{Y^{4-}} \longrightarrow \mathrm{[MY]^{n-4}}$$

$$K_f = \frac{[MY]^{n-4}}{[M^{n+}][Y^{4-}]} \tag{7}$$

The stability constants of these EDTA-metal complexes indicate how stable they are. A fairly large stability constant indicates that there is a strong tendency for that metal ion to complex with EDTA. Stability constants of the evaluated metal ions and their reactions with EDTA are summarized in Table 5.

Table 5. The formation constants of various metal ions.

Metal cation	Log K_f
Cu^{2+}	18.80
Ni^{2+}	18.62
Mn^{2+}	14.04
Al^{3+}	16.13
Fe^{3+}	25.10
Na^{+}	1.66
Ca^{2+}	10.70
Mg^{2+}	8.69

As illustrated above, the stability constants of EDTA complexes of Cu^{2+}, Ni^{2+}, Al^{2+}, Mn^{2+} and Fe^{2+} ions are higher than the stability constants of EDTA complexes of Ca^{2+} and Mg^{2+} ions. Thus, when a μPAD is titrated for the determination of Ca^{2+} and Mg^{2+} in the presence of the metal ions mentioned, EDTA would complex with them preferentially affecting the expected results. When the concentrations of these interfering ions is similar to or greater than EDTA, IT would allow uncomplexed Ca^{2+} and Mg^{2+} ions to react with the indicator in the detection zones.

Figure 21 shows the minimum pH required for various metals to form a complex with EDTA. As shown, the minimum pH that is needed by many metal ions is lower than pH 10. Thus, all metal ions shown in Figure 21 can complex with EDTA at pH 10, and are expected to interfere with detection. Further, these metal ions could also react with the indicator which would also lead to false positive results.

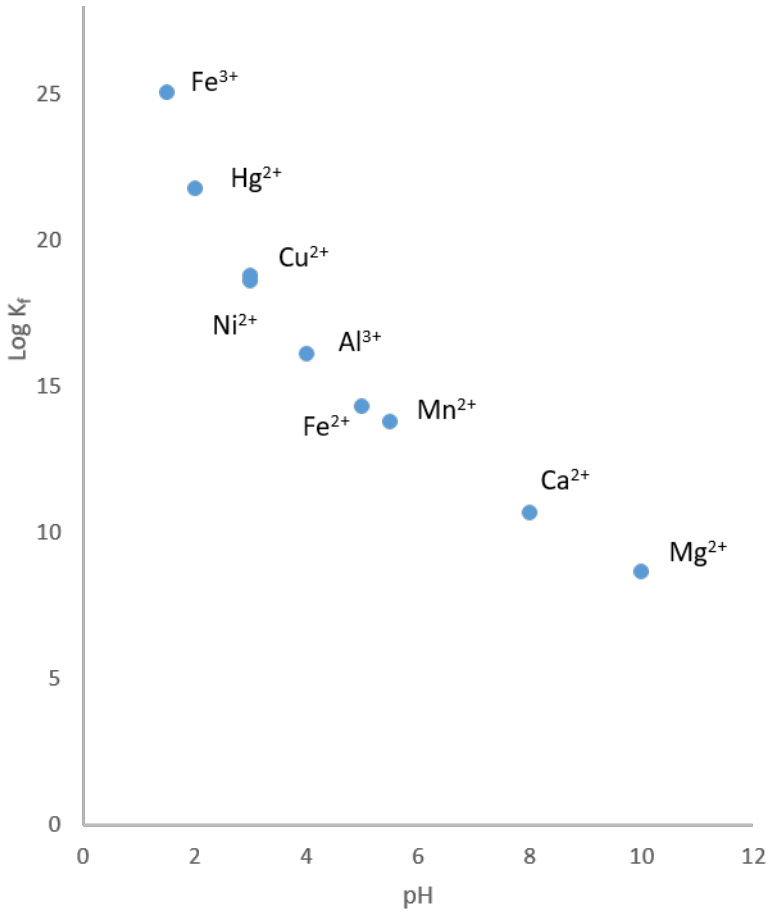

Figure 21. Minimum pH required for various metals to form a complex with EDTA.[1]

3.12 Interference analysis

To determine if Cu^{2+}, Ni^{2+}, Al^{2+}, Mn^{2+} and Fe^{2+} ions interfere with the total water hardness determination, μPADs made for pH 10 were titrated using solutions of these ions with known concentrations.

Row 1 in Table 6 shows the four titrated μPADs, with various concentrations of Cu^{2+} solutions. As shown in the first row, the titrated μPAD with 1 mM Cu^{2+} solution, only the detection zone adjacent to 0 mM EDTA turned pink, while all other nine detection zones remained blue.

This result indicates that, even at 1 mM level, Cu^{2+} ions bind with EBT providing a false positive and interfering with the evaluation of total hardness of water. As shown in Table 6 also shows the titrated μPAD with 10 mM, 50 mM and 100 mM of Cu^{2+} solutions respectively, and few or all detection zones changed the color to pink, confirming Cu^{2+} ions interfere in this μPAD titration.

As shown in Table 6, when Ni^{2+} solutions were titrated the color change is visible in detection zones at 0 and 10 mM regions. These results indicate that nickel is also an interference for the hard water analysis.

Also Fe^{3+} solutions were titrated with μPADs using several solutions of known concentrations. The titrated μPAD with 1 mM Fe^{3+} solution, only the detection zone adjacent to 0 mM EDTA turned pink, while all other nine detection zones remained blue. With all other concentrations, some detection zones changed color. This result indicates that at 1 mM level or above Fe^{3+} ions could bind with EBT indicator providing a false positive results and interfering with the evaluation of total hardness of water.

Table 6. μPADs results for various known concentrations of Cu^{2+}, Ni^{2+}, Al^{2+}, Mn^{2+} and Fe^{3+} ions.

Metal	1 mM	10 mM	50 mM	100 mM
Cu^{2+}	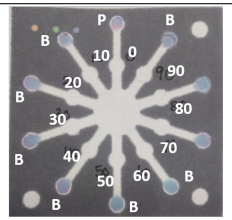	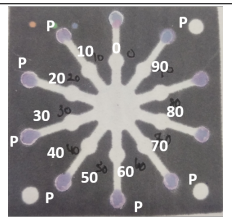	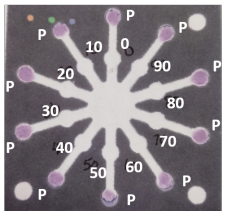	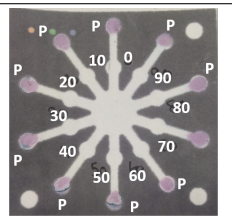
Ni^{2+}	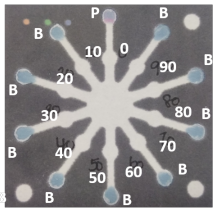	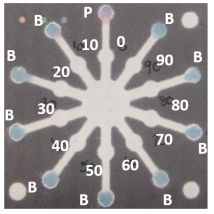	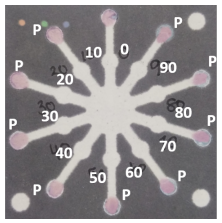	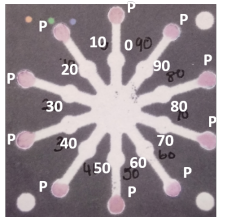
Mn^{2+}	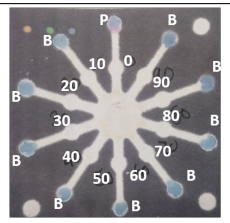	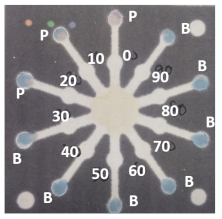	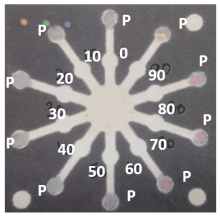	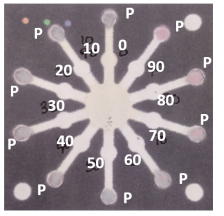
Fe^{3+}	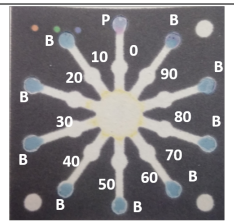	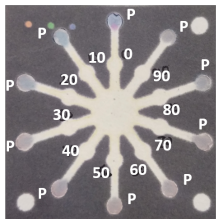	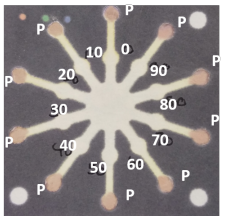	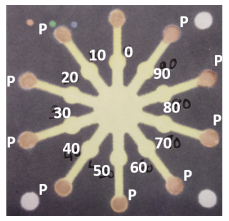
Al^{3+}	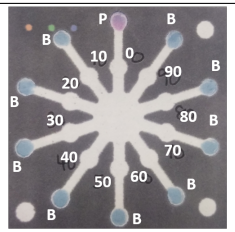	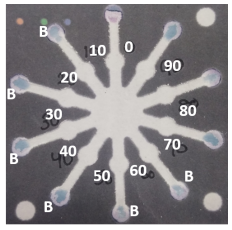	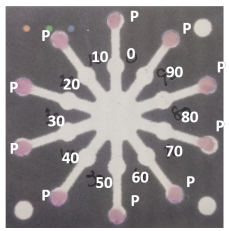	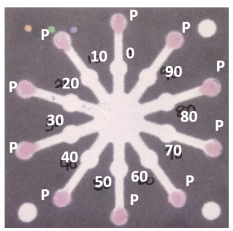

When a μPAD was titrated with 1 mM Mn^{2+} solution, only the detection zone adjacent to 0 mM EDTA turned pink, while all other nine detection zones remained blue. Further, as shown in Table 6, with all other Mn^{2+} concentrations, few or all detection zones change color. These results indicate that at 1 mM level or above, Mn^{2+} ions could bind with EBT indicator providing a false positive result and interfere with the evaluation of total hardness of water.

When the Al^{3+} solutions were titrated using the μPADs with 1 mM Al^{3+} solution, the detection zone adjacent to 0 mM EDTA turned pink, while all other nine detection zones remained blue. With all other concentrations, few or all detection zones changes color. These results indicate that at 1 mM level or above, Al^{3+} ions could bind with EBT indicator providing a false positive result and interfere with the evaluation of total hardness of water. In summary, it was found that Cu^{2+}, Ni^{2+}, Al^{2+}, Mn^{2+} and Fe^{2+} ions when present in natural waters can interfere with the total water hardness determination.

CHAPTER FOUR: CONCLUSIONS AND FUTURE DIRECTIONS

Since the introduction of microfluidic paper based devices in 2007, they have become a promising, easy to use and cost effective alternative to complicated and expensive instruments. In this project, the classic titration for water hardness analysis was adapted to microfluidic paper based devices. These μPADs are capable of providing quantitative total hardness as well as concentrations of Ca^{2+} and Mg^{2+} ions of unknown water samples.

In order to create functioning μPADs, several parameters involved in the development of the μPADs were studied and optimized including wax melting temperature, the melting time, the optimum barrier width, and the channel width. Using the optimized parameters, μPADs for hard water analysis were designed and optimized.

Then, they were used for testing calcium and magnesium ion concentrations of using real world samples. In order to confirm that the results obtained from the μPADs are accurate, ICP - OES analysis on the some real world samples was conducted. It was determined that the results obtained from the μPADs are fairly accurate.

Also several other metal cations were evaluated for possible interferences (Fe^{3+}, Cu^{2+}, Ni^{2+}, Mn^{2+} and Al^{3+}). It was discovered that these metals can interfere with the μPAD analysis.

In summary, low-cost and simple to-use paper based analytical devices were successfully developed which are capable of quantitatively analyze calcium and magnesium ions in a mixture. In water, not only calcium and magnesium ions, but also other metal ions including Fe^{3+}, Cu^{2+}, Ni^{2+}, Mn^{2+} and Al^{3+} could be present, which could raise significant health and environmental issues. Thus, microfluidic paper based devices can be further developed to quantify the presence of these metal ions as a low cost lab-on-a-chip type portable devices.

REFERENCES

[1] Skoog, D. A.; West, D. M.; Holler, F. J.; Crouch, S. R. *Fundamentals of Analytical Chemistry*; Cengage Learning, **2013**.

[2] World Health Organization: United Nations International Children′s Emergency Fund, Progress on Drinking Water and Sanitation. **2012**, 1–66.

[3] Anderson, T. W.; Talbot, F. D. F. Ischemic Heart Disease, Water Hardness and Myocardial Magnesium. **1975**, *113*, 199–203.

[4] Idaura, R. U. Y. L. O. Magnesium Intake and Risk of Type 2. *Diabetes Care* **2004**, *34*, 2116–2122.

[5] Miyake, Y.; Yokoyama, T.; Yura, A.; Iki, M.; Shimizu, T. Ecological Association of Water Hardness with Prevalence of Childhood Atopic Dermatitis in a Japanese urban area. *Environ. Res.* **2004**, *94*, 33–37.

[6] Wigle, D.T.; Mao, Y.; Semenciw , R.; Smith, M.H.; Toft, P. Contaminants in Drinking Water and Cancer Risks in Canadian Cities. *Can J Public Heal.* **1986**, *77*, 335–342.

[7] Almeida, M. I. G. S.; Jayawardane, B. M.; Kolev, S. D.; Mckelvie, I. D. Developments of Microfluidic Paper-Based Analytical Devices (μPADs) for Water Analysis : A review. *Talanta* **2017**, *177*, 176–190

[8] Yamada, K.; Henares, T. G.; Suzuki, K.; Citterio, D. Paper-Based Inkjet-Printed Microfluidic Analytical Devices. *Angew. Chemie Int. Ed.* **2015**, *54*, 5294–5310.

[9] Zhang, Y.; Zhou, C.; Nie, J.; Le, S.; Qin, Q.; Liu, F.; Li, Y.; Li, J. Equipment-Free Quantitative Measurement for Microfluidic Paper-Based Analytical Devices Fabricated Using the Principles of Movable- Type Printing. **2014**, *86*, 2005–2012

[10] Stock, R.; Rice, C. *Chromatographic Methods*, 3rd ed. John Wiley & Sons: New York, **1974**, 106-110.

[11] Li, X.; Tian, J. ;Garnier, G.; Shen, W. Fabrication of Paper-Based Microfluidic Sensors by Printing. *Colloids Surfaces B Biointerfaces* **2010**, *76*, 564–570.

[12] Mazeau, K. *Conformations, Structures, and Morphologies of Celluloses in Polysaccharides: Structural Diversity and Functional Versatility*, 2nd ed. CRC Press:Florida, **2005**, 41–69.

[13] Chem, J. M.; Credou, J.; Berthelot, T. Cellulose : from Biocompatible to Bioactive Material. *J. Mater. Chem.* **2014**, *2*, 4767–4788.

[14] Moon, R. J.; Martini, A.; Nairn, J.; Simonsen, J. ; Youngblood, J. Cellulose Nanomaterials Review: Structure, Properties and Nanocomposites. *Chem. Soc. Rev.* **2011**, *40*, 3941-3994.

[15] Klemm, D.; Heublein, B.; Fink, H. P.; Bohn, A. Cellulose: Fascinating Biopolymer and Sustainable Raw Material. *Angew. Chemie - Int. Ed.* **2005**, *44*, 3358–3393.

[16] Sahin, H. T.; Arslan, M. B. A Study on Physical and Chemical Properties of Cellulose Paper Immersed in Various Solvent Mixtures. *Int. J. Mol. Sci.* **2008**, *9*, 78–88.

[17] Pelton, R. Bioactive Paper Provides a Low-cost Platform for Diagnostics. *Trends Anal. Chem.* **2009**, *28*, 925–942.

[18] Free, A. H.; Adams, E. C.; Kercher, M. L.; Helen, M.; Cook, M. H. Simple Specific Test for Urine Glucose. *Clin. Chem* **1956**, *3*, 163–168.

[19] Lopez-ruiz, N.; Curto, V. F.; Erenas, M. M.; Benito-lopez, F.; Diamond, D.; Palma, A. J.; Capitan-vallvey, L. F. Smartphone-Based Simultaneous pH and Nitrite Colorimetric Determination for Paper Microfluidic Devices. *Anal.Chem.* **2014**, *86*, 9554-9562

[20] Santhiago, M.; Henry, C.S.; Kubota, L. Low Cost, Simple Three Dimensional Eelectrochemical Paper Based Analytical Device for Determination of p-nitrophenol. *Electrochim. Acta* **2014**, *130*, 771-777.

[21] Ortiz-Gomez, I.; Ortega-Munoz, M.; Salinas-Castillo, K. Alvarez-Bermejo, J.; Ariza-Avidad, M.; de Orbe-Paya, I.; Santoyo-Gonzalez, F.; Capitan-Vallvey, L. Tetrazine-Based Chemistry for Nitrite Determination in a Paper Microfluidic Device. *Talanta* **2016**, *160*, 721-728.

[22] Sicard, C.; Glen, C.; Aubie, B.; Wallace, D.; Jahanshahi-Anbuhi, S.; Pennings, K.; Daigger, G.T.; Pelton, R.; Brennan, J.D.; Filipe, C. Tools for Water Quality Monitoring and Mapping Using Paper-Based Sensors and Cell Phones,. *Water Res.* **2015** *70*, 336-341.

[23] Chen, G.H.; Chen, W.Y.; Yen, Y.C.; Wang,C.W.; Chang, H.T.Chen, C. Detection of Mercury(II) Ions Using Colorimetric Gold Nanoparticles on Paper-Based Analytical Devices. *Anal. Chem.* **2014**, *86*, 6843–6849.

[24] Pla-Tolós, J.; Moliner-Martínez, Y.; Verdú-Andrés, J.; Casanova-Chafer, J.; MolinsLegua, C.;Campíns-Falcó, P. New Optical Paper Sensor for in Situ Measurement of Hydrogen Sulphide in Waters and Atmospheres. *Talanta* **2016**, *156*, 79-86.

[25] Jayawardane, B.M.; McKelvie, I.D.; Kolev, S. Development of a Gas-Diffusion Microfluidic Paper-Based Analytical Device (PAD) for the Determination of Ammonia in Wastewater Samples. *Anal. Chem.* **2015**, *87*, 4621-4626.

[26] Martinez, A.W.; Phillips, S.T.; Carrilho, E.; Thomas, S.W.; Sindi, H.; Whitesides, G. Simple Telemedicine for Developing Regions: Camera Phones and Paper-Bbased Microfluidic Devices for Real-time, off-site Diagnosis. *Anal. Chem.* **2008**, *80*, 3699-3707.

[27] Dungchai, W.; Chailapakul, O.; Henry, C. S. A Low-Cost, Simple, and Rapid Fabrication

Method for Paper-Based Microfluidics Using Wax Screen-Printing. *Analyst* **2011**, *136*, 77–82.

[28] Abe, K.; Suzuki, K.; Citterio, D. Inkjet-printed Microfluidic Multianalyte Chemical Sensing Paper. *Anal. Chem.* **2008**, *80*, 6928–6934.

[29] Hossain, S. M. Z.; Brennan, J. D. β-Galactosidase-Based Colorimetric Paper Sensor for Determination of Heavy Metals. *Anal. Chem.* **2011**, *83*, 8772–8778.

[30] Maejima, K.; Tomikawa, S.; Suzuki, K.; Citterio, D. Inkjet Printing: an Integrated and Green Chemical Approach to Microfluidic Paper-Based Analytical Devices. *RSC Adv.* **2013**, *3*, 9258-9263.

[31] Yamada, K.; Takaki, S.; Komuro, N. ;Suzuki, K.; Citterio, D. An Antibody-free Microfluidic Paper-Based Analytical Device for the Determination of Tear Fluid Lactoferrin by Fluorescence Sensitization of Tb^{3+}. *Analyst* **2014**, *139*, 1637-1643.

[32] Wu, Y.; Xue, P.; Kang, Y.; Hui, K. M. Paper-Based Microfluidic Electrochemical Immunodevice Integrated with Nanobioprobes onto Graphene Film for Ultrasensitive Multiplexed Detection of Cancer Biomarkers. *Anal. Chem.* **2013**, *85*, 8661–8668.

[33] A.W.Martinez, S. T.; Phillips, M. B.; G.M.Whitesides, Patterned Paper as a Platform for Inexpensive, Low-Volume, Portable Bioassay. *Angew. Chem., Int. Ed.* **2007**, *46*, 1318–1320.

[34] Carrilho, E.; Martinez, A. W.; Whitesides, G. M. Understanding Wax Printing: a Simple Micropatterning Process for Paper-Based Microfluidics. *Anal. Chem.* **2009**, *81*, 7091-7095.

[35] Nery, E. W.; Kubota, L. T., Sensing Approaches on Paper-Based Devices: a Review. *Anal Bioanal. Chem.* **2013**, *405*, 7573-7595.

[36] Dungchai, W.; Chailapakul, O.; Henry, C. S. Use of Multiple Colorimetric Indicators for Paper-Based Microfluidic Devices. *Anal. Chim. Acta* **2010**, *674*, 227–233.

[37] Nie, Z.; Deiss, F.; Liu, X.; Akbulut, O.; Whitesides, G. M. Integration of Paper-Based Readers Microfluidic Devices with Commercial Electrochemical. *Lab Chip* **2010**, *10*, 3163-3169.

[38] Yetisen,A. K.; Akram, M. S ; Lowe, C. R. Paper-Based Microfluidic Point-of-care Diagnostic Devices. *Lab Chip* **2013**, *13*, 2210–51.

[39] Wang, X.R.; Li, B.W.; You, H.Y.; Chen, L. An Ion Imprinted Polymers Grafted Paperbased Fluorescent Sensor Based on Quantum Dots for Detection of Cu^{2+} Ions. *Chin. J. Anal. Chem.* **2015**, *43*, 1499-1504.

[40] Chen, X.; Yu, S.; Yang, L.; Wang, J.; Jiang, C. Fluorescence and Visual Detection of Fluoride Ions Using a Photoluminescent Graphene Oxide Paper Sensor. *Nanoscale* **2016**, *8*, 13669-13677.

[41] Wang, X.; Li, B.W.; You, H.Y.; Chen, L. An Ion Imprinted Polymers Grafted Paper-Based Fluorescent Sensor Based on Quantum Dots for Detection of Cu^{2+} ions. *Chin. J. Anal. Chem.* **2015**, *43*, 1499–1504.

[42] Petryayeva, E.; Algar, W. Proteolytic Assays on Quantum-dot-Modified Paper Substrates Using Simple Optical Readout Platforms. *Anal. Chem.* **2013**, *85*, 8817-8825.

[43] Li, X.; Ballerini, D. R. ; W. Shen, W. A Perspective on Paper-Based Microfluidics: Current Status and Future Trends. *Biomicrofluidics* **2012**, *6*, 11301–11311,.

[44] Martinez, A. W.; Phillips, S. T.; Whitesides, G. M.; Carrilho, E. Diagnostics for the Developing World: Microfluidic Paper-Based Analytical Devices. *Anal. Chem.* **2010**, *82*, 3–10.

[45] Yang, X.; Forouzan, O.; Brown, T. P.; Shevkoplyas, S. S. Integrated Separation of Blood Plasma from Whole Blood for Microfluidic Paper-Based Analytical Devices. *Lab Chip* **2012**, *12*, 274–80.

[46] Mentele, M. M.; Cunningham, J.; Koehler, K.; Volckens, J.; Henry, C. S. Microfluidic Paper-Based Analytical Device for Particulate Metals. *Anal.Chem.* **2012**, *84*, 4474-4480

[47] Evans, E.; Gabriel, E. F. M.; Coltro, W. K. T.; Garcia, C. D. Rational Selection of Substrates to Improve Color Intensity and Uniformity on Microfluidic Paper-Based Analytical Devices. *Analyst* **2014**, *139*, 2127-2132.

[48] Birch, N.C.; Stickle, D. Example of Use of a Desktop Scanner for Data Acquisition in a Colorimetric Assay. *Clin. Chim. Acta* **2003**, *333*, 95–96.

[49] Jayawardane, B. M. Wongwilai, W. Grudpan, K. Kolev, S. D. Heaven, M. W. Nash, D. M.; McKelvie, I. D. Evaluation and Application of a Paper-Based Device for the Determination of Reactive Phosphate in Soil Solution. *J. Environ. Qual.* **2014**, *43*, 1081-1085.

[50] Orna, M. V. *The Chemical History of Color*; Springer Berlin Heidelberg: Berlin, Heidelberg, **2013**.

[51] World Health Organization, *Nitrate and nitrite in drinking-water, Background Document for Development of WHO Guidelines for Drinking-Water quality*; **2011**.

[52] Cardoso, T.M.G.; Garcia,P.T.; Coltro, W. Colorimetric Determination of Nitrite in Clinical, Food and Environmental Samples Using Microfluidic Devices Stamped in Paper Platforms. *Anal. Methods* **2015**, *7*, 7311 –7317.

[53] Jayawardane, B.M.; Wei,S.; McKelvie, I.D.; Kolev, S. Microfluidic Paper-Based Analytical Device for The Determination of Nitrite and Nitrate. *Anal. Chem.* **2014**, *86*, 7274 –7279.

[54] Jayawardane, B.M.; Wongwilai, W.; Grudpan, K.; Kolev, S.D.; Heaven, M.; Nash, D.M.; McKelvie, I. Evaluation and Application of a Paper-Based Device for The Determination of Reactive Phosphate in Soil Solution. *J. Environ. Qual.* **2014**, *43*, 1081 –1085.

[55] Jayawardane, B.M.; McKelvie, I.D.; Kolev, S. A Paper-Based Device for Measurement of Reactive Phosphate in Water. *Talanta* **2012**, *100*, 454 –460.

[56] Lin, Y. ; Gritsenko, D.; Feng, S.; Chen, Y.; Lu, X.; Xu, J. Detection of Heavy Metal by Paper-Based Microfluidics. *Biosens. Bioelectron.* **2016**, *83*, 256–266.

[57] Leermakers, M. ; Baeyens, W. ; Quevauviller, P.; Horvat, M. Mercury in Environmental Samples: Speciation, Artifacts and Validation. *TrAC - Trends Anal. Chem.* **2005**, *24*, 383–393.

[58] Zhang, M.; Ge, L.; Ge, S.G.; Yan,M.; Yu,J.H.; Huang,J.D.; Liu, S. Three-Dimensional Paper-Based Electrochemiluminescence Device for Simultaneous Detection of Pb^{2+} and Hg^{2+} Based on Potential-Control technique. *Biosens. Bioelectron.* **2013**, *41*, 544 –550.

[59] Guo, J.F. ; Huo, D.Q. ; Yang, M. ; Hou, C.J.; Li, J.J.; Fa, H.B.; Luo, H.B. ; Yang, P. Colorimetric Detection of Cr (VI) Based on The Leaching of Gold Nanoparticles Using a Paper-Based Sensor. *Talanta* **2016**, *161*, 819-825.

[60] Alahmad, W. ; Uraisin, K.; Nacapricha, D. ; Kaneta, T. A Miniaturized Chemiluminescence Detection System for a Microfluidic Paper-Based Analytical Device and Its Application to the Determination of Chromium(III). *Anal. Methods* **2016**, *8*, 5414-5420.

[61] Li, M.S.; Cao, R.; Nilghaz, A.; Guan, L.Y. ; Zhang, X.W. ; Shen, W. "Periodic-Table-Style" Paper Device for Monitoring Heavy Metals in Water. *Anal. Chem.* **2015**, *87*, 2555-2559.

[62] Jayawardane, B.M. ; Coo, L. ; Cattrall, R.W. ; Kolev, S. The Use of aPolymer Inclusion Membrane in a Paper-Based Sensor for The Selective Determination of Cu(II). *Anal. Chim. Acta* **2013**, *803*, 106 –112.

[63] Ratnarathorn, N.; Chailapakul, O. ; Henry, C.S. ; Dungchai, W. Simple Silver Nanoparticle Colorimetric Sensing for Copper by Paper-Based Devices. *Talanta* **2012**, *99*, 552 –557.

[64] Chaiyo, S. ; Siangproh, W. ; Apilux, A. ; Chailapakul, O. Highly Selective and Sensitive Paper-Based Colorimetric Sensor using Thiosulfate Catalytic Etching of Silver Nanoplates for Trace Determination of Copper Ions. *Anal. Chim. Acta* **2015**, *866*, 75 –83.

[65] Chaiyo, S.; Apiluk, A.; Siangproh, W. ; Chailapakul, O. High Sensitivity and Specificity Simultaneous Determination of Lead, Cadmium and Copper Using PAD with Dual Electrochemical and Colorimetric Detection. *Sens. Actuator B-Chem.* **2016**, *233*, 540 –549.

[66] Eaton, A.D.; Clesceri, L.S.; Greenberg, A. E.; Franson, H.M., Part 3000 - Metals, in:, Standard Methods for The Examination of Water & wastewater. American Public Health Association: Washington, DC **2012**.

[67] Ujawar, L. H. M.; Elemban, A. A. F.; Hahawi, M. S. E. L. Hexamethyldisilazane Modified Paper as an Ultra-sensitive Platform for Visual Detection of Hg^{2+}, Co^{2+}, Zn^{2+} and the Application to Semi-quantitative Determination of Hg^{2+} in Wastewater. *Anal. Sci.* **2016**, *32*, 491–497.

[68] Shi, J.J. ; Tang, F. ; Xing, H.L.; Zheng, H.X. ; Bi,L.H. ; Wang, W. Electrochemical Detection of Pb and Cd in Paper-Based Microfluidic Devices. *J. Braz. Chem. Soc.* **2012**, *23*, 1124 –1130.

[69] Karita, S. ; Kaneta, T. Chelate Titrations of Ca^{2+} and Mg^{2+} Using microfluidic Paper-Based Analytical Devices. *Anal. Chim. Acta* **2016**, *924*, 60–67.

[70] Dos Santos, A. J.; De Lima, M. D.; Da Silva, D. R.; Garcia-Segura, S. Martínez-Huitle, C. A. Influence of The Water Hardness on The Performance of Electro-Fenton Approach: Decolorization and Mineralization of Eriochrome Black T. *Electrochim. Acta* **2016**, *208*, 156–163.

[71] Sengupta, P. Potential Health Impacts of Hard Water. *Int J Prev Med.* **2013**, *4*, 866–875.

[72] Douglas, B.; McDaniel, D. ; Alexander, J. *Concepts and Models of Inorganic Chemistry*, 3rd ed. John Wiley & Sons, Inc, **1993**; p 384–389.

[73] Harris, D. *Quantitative Chemical Analysis*, 8th ed.; W.H. Freeman and Company, **2010**; p 236–253.

[74] Schmid, R. W. ; Reilley, C. N. New Complexon for Titration of Calcium in the Presence of Magnesium. *Anal. Chem.* **1957**, *29*, 264–268.

[75] Cai, L.; Fang, Y.; Mo, Y.; Huang, Y.; Xu, C.; Zhang, Z.; Wang, M. Visual Quantification of Hg on a Microfluidic Paper-Based Analytical Device Using Distance-Based Detection Technique. *AIP Adv.* **2017**, *7*, 85214 – 85218.

[76] Picha, K.; Spackman, C.; Samuel, J. Droplet Spreading Characteristics Observed During 3D Printing of Aligned Fiber-Reinforced Soft Composites. *Addit. Manuf.* **2016**, *12*, 121–131.

[77] Cunha, A. G. ; Gandini, A. Turning Polysaccharides into Hydrophobic Materials: A Critical Review. Part 1. Cellulose. *Cellulose* **2010**, *17*, 875–889.

[78] Ray, B. ; Bartell, F. E. Hysteresis of Contact angle of Water on Paraffin.Ph.D thesis, **1952**.

[79] Cate, D. M. ; Adkins, J. A.; Mettakoonpitak, J.; Henry, C. S. Recent Developments in Paper-Based Microfluidic Devices. *Anal. Chem.* **2015**, *87*, 19–41.

[80] Harris, D. C. *Exploring Chemical Analysis*, 5th ed. W. H. Freeman: New York. **2012**.